

## Oscillatory flow past a circular cylinder in a rotating frame

By M. D. KUNKA<sup>1</sup> AND M. R. FOSTER<sup>2</sup>

<sup>1</sup>Department of Mathematics,

<sup>2</sup>Department of Aerospace Engineering, Applied Mechanics and Aviation,  
The Ohio State University, Columbus, OH, 43210, USA

(Received 1 July 1996 and in revised form 16 December 1996)

Because of the importance of oscillatory components in the oncoming flow at certain oceanic topographic features, we investigate the oscillatory flow past a circular cylinder in an homogeneous rotating fluid. When the oncoming flow is non-reversing, and for relatively low-frequency oscillations, the modifications to the equivalent steady flow arise principally in the ‘quarter layer’ on the surface of the cylinder. An incipient-separation criterion is found as a limitation on the magnitude of the Rossby number, as in the steady-flow case. We present exact solutions for a number of asymptotic cases, at both large frequency and small nonlinearity. We also report numerical solutions of the nonlinear quarter-layer equation for a range of parameters, obtained by a temporal integration. Near the rear stagnation point of the cylinder, we find a generalized velocity ‘plateau’ similar to that of the steady-flow problem, in which all harmonics of the free-stream oscillation may be present. Further, we determine that, for certain initial conditions, the boundary-layer flow develops a finite-time singularity in the neighbourhood of the rear stagnation point.

---

### 1. Introduction

A number of important biological and physical phenomena are peculiar to large oceanic seamounts. There is ample evidence of the physical effects in the literature: Owens & Hogg (1980), Huppert & Bryan (1976) and Gould, Hendry & Huppert (1981) all show flow effects due to the topography, some of which can be reasonably well modelled by some simple baroclinic theories. However, there is some recent evidence of significant impact on seamount-surface fauna that is particular to the seamount environment (Genin *et al.* 1986). It is sometimes the case that seamounts are imbedded in oscillatory currents because of significant tidal components to the circulation in the seamount neighbourhood. However, the greatest part of the literature on theoretical and laboratory modelling of such flows considers only objects in steady streams. (See, for example, Hogg 1973; Baines & Davies 1980; Boyer, Davies & Holland 1984; Boyer *et al.* 1987; Foster 1989.)

Apart from some earlier work by Huppert & Bryan (1976) incorporating some effects of unsteadiness, there has been more recent activity on the effects of oscillatory flows near seamounts, or their laboratory representations. Verron (1986) found both localized near-seamount effects and also significant effects on seamount wake signatures from unsteadiness in the oncoming flow. Such effects have also been seen in the laboratory studies of Boyer & Zhang, for idealized shapes (1990*b*) and for a

more realistic seamount geometry as well (1990a). Effects of cross-stream oscillation have been investigated by Xu, Boyer & Zhang (1993), with effects of stratification – not directly relevant to the present investigation – explored in a series of experiments by Zhang & Boyer (1993). Rectified currents, when oscillatory components in the oncoming flow induce steady circulations, arise in many of these laboratory situations. The papers of Boyer and his co-workers that are of most relevance to the work reported here are Boyer & Zhang (1990b) and Boyer *et al.* (1991), though the former concentrates on the wake signatures that arise at Rossby numbers larger than those considered here.

As a way of beginning on the theoretical questions involving unsteadiness at a seamount, we explore in this paper the homogenous rotating flow past an idealized shape for the case when the oncoming stream has an oscillatory component but is non-reversing. We know from the spectrum of, say, the Feiberling Guyot (P. Lonsdale 1988, personal communication), that there are a variety of frequencies that are important. The obvious dimensionless parameter is  $\omega'/\Omega$ , where  $\omega'$  is the oscillation frequency and  $\Omega$  is the rotation rate of the frame of reference. In this paper, we explore two portions of the frequency range in which modifications due to unsteadiness occur principally in the surface boundary layer of the obstacle. Since the seminal experiments of Taylor (1923, for example), it has been evident that Coriolis forces can delay breakaway of the boundary layer from the surface to relatively large Reynolds numbers – far beyond the critical Reynolds numbers for separation in non-rotating flows. How does an oscillatory component alter that behaviour? For the greater part of the paper, we consider quite low frequencies, i.e.  $\omega'/\Omega$  of the order of the half-power of the Ekman number. We discover the conditions under which the flow first breaks away from the surface. Later in the paper, we investigate the flow for  $\omega' = O(\Omega)$ , but only for a cylinder that spans the entire depth of the fluid layer. It is clear from P. Lonsdale (1988, personal communication) that there are significant time scales from a few hours to times of several days – so it is not unreasonable to examine the low-frequency modes as well as the more obvious choice  $\omega' = O(\Omega)$ . The most interesting scenario, which is beyond the scope of the present work, is one in which there is nonlinear interaction of the currents due to the dominant frequencies in the spectrum.

In a related problem from the study of the flow of electrically conducting fluids, Leibovich (1967) and Buckmaster (1969) found a criterion for separation for flow at high Reynolds number past a circular cylinder. Walker & Stewartson (1972, 1974) related this problem to the problem of flow past a circular cylinder and then a hemisphere in a rapidly rotating frame of reference. Their analysis of the rotating-flow problem rests on a sequence of papers that dealt with the boundary- and shear-layer structures in these flows. (See Proudman 1956; Stewartson 1957, 1966; Jacobs 1964 and Moore & Saffman 1969, for example.)

Rather than the Reynolds number, it is more convenient to work with the Rossby number,  $\epsilon \equiv U/\Omega h$ , and the Ekman number,  $E \equiv \nu/\Omega h^2$ , where  $\nu$  is the kinematic viscosity,  $U$  is the fluid velocity scale from the flow far from the bump,  $h$  is the layer depth and the object imbedded in the flow has radius  $ah$ . Both  $\epsilon$  and  $E$  can be quite small in oceanic settings. (See, for example, Boyer *et al.* 1991.) The Reynolds number is then  $\epsilon/Ea$ . The parameter which is important in characterizing the flow separation phenomenon is  $\lambda \equiv \epsilon/(aE^{1/2})$ ; Walker & Stewartson (1972) found incipient boundary-layer separation at  $\lambda = 1$ .

The boundary layer on the vertical cylinder wall, the familiar ‘quarter layer’, is nonlinear and hence solutions must in general be found numerically; however, there

are self-similar solutions of these equations valid near the forward and rear stagnation points on the cylinder. In the context of the MHD problem, both Leibovich (1967) and Buckmaster (1969) found that, while there is no difficulty with the forward stagnation point, there are interesting things happening at the rear location: for  $\lambda < 1/2$ , solutions to the similarity equation exist, but for  $\lambda > 1$ , the shear stress is negative and the boundary layer presumably leaves the surface. For  $1/2 < \lambda < 1$ , no similarity solution can be found that satisfies the edge velocity condition, but the appropriate solution asymptotes instead to what we shall refer to as a ‘plateau’ velocity: an extensive flat portion of the velocity profile, in the middle of the boundary layer. Unable to find the solution that connects this flat plateau-like behaviour to actual edge velocity, both Buckmaster and Leibovich speculated that some unsteadiness or other complexity occurs in the range  $1/2 < \lambda < 1$ .

Walker & Stewartson (1972, 1974) found that in the (related) rotating flow problem there is no difficulty whatever in obtaining the numerical solution of the quarter-layer equation all the way to the rear stagnation point so long as  $\lambda < 1$ . Page (1985) reported that, indeed, the similarity equations have solutions for all  $\lambda < 1$ , but flow near the rear stagnation point is not completely described by the similar solution if  $1/2 < \lambda < 1$ . Finally, Page & Cowley (1988) determined that in this latter range, the boundary layer near the rear stagnation point has a steady three-zone structure; the similarity equations describe the innermost region, including the plateau region noted above (Leibovich 1967; Buckmaster 1969).

As noted above, we explore in this paper the effects of upstream temporal oscillation on the flow past a large cylindrical obstacle. (‘Large’ here means only that the cylinder is tall enough to protrude through the benthic boundary layer, occupying a significant portion of the fluid layer.) The cylinder need not extend from the bottom to the top of the fluid layer for the low-frequency analysis presented here to be valid (Foster 1972). Therefore, we take the far-upstream velocity to be

$$U(1 + \gamma \cos(\omega t));$$

$\gamma$  is a constant and  $\omega$  is a non-dimensional frequency,  $\omega = (\omega'/\Omega)/E^{1/2}$ . Throughout this paper, we take the upstream flow to be non-reversing, so that  $|\gamma| < 1$ . There is some experimental work (Hudspeth 1991) that suggests that the parameter of greatest significance in such oscillatory flows is the Keulegan-Carpenter parameter, which is  $K = U/(\omega'ah)$ . For the case when  $\omega = O(1)$ , this quantity is also  $O(1)$ , since  $K = \lambda/\omega$ . So, at these small Rossby numbers,  $\lambda = O(1)$  seems the critical order from the experiments as well. (The importance of  $K$  was first noted in the seminal paper by Keulegan & Carpenter 1958.)

The goal of this particular analysis is to inquire into the nature of the breakdown in the boundary-layer flow that leads to breakaway of the layer from the surface, and in particular to determine the critical value for  $\lambda$  as a function of  $\gamma$ . In §2 of the paper, we formulate the boundary-layer problem, and in §3 we construct the (regular) perturbation problem for small  $\lambda$ , and also an asymptotic solution for large  $\omega$ .

In §4, we investigate the self-similar structure near the rear stagnation point, where breakaway begins; we find an extremely complicated behaviour of the solution there, recovering for  $\gamma \rightarrow 0$  the plateau velocity seen in the steady problem and its generalization as a long-time periodic plateau, if  $\gamma = O(1)$ . We also determine that, for a general initial-value problem for the edge velocity, the periodic plateau is not always the long-time limit. There may be a breakdown at a finite time that moves the flow to a quite different state.

In §5, we formulate the full finite-difference problem for the boundary-layer equa-

tion, and solve it with a time integration, to determine the critical  $\lambda(\gamma, \omega)$ . Solutions there are compared near the rear stagnation point with the self-similar results from §4; in general, the agreement is excellent, though we find the detailed determination of critical  $\gamma$  to be extremely sensitive to truncation error in the time – space integration.

We briefly present the results for the case  $\omega' = O(\Omega)$  in §6. We find the same splitting of the layer into an outer quarter layer and an inner Stokes layer – this time of width  $E^{1/2}$  – as is found for the large- $\omega$  case of §3. However, these results are limited to cylinders that span the entire distance from one plate to another.

The ‘rectification’ phenomenon, i.e. the transfer of energy from the oscillation to the steady anticyclonic motion around the obstacle, which has been explored by Boyer and colleagues, is not in evidence here. Zimmerman’s (1980) results indicate that it is vortex stretching that produces rectification. The only vortex stretching occurring in this parameter range arises in the quarter layer, and it is very weak, being related to the Ekman outflow. Hence, it is not surprising that there is no rectification here.

There are questions related to the general initial-value problem not thoroughly investigated in this paper; what we have shown is that there are time-periodic solutions to the equations of motion for  $\lambda < 1$ . We do know that the time-periodic solutions found here are stable, but we do not yet know the full extent of their domain of attraction; that must await a subsequent paper.

However, analysis of the start-up of a cylinder from rest to a state of uniform motion has been reported by Stocker, Duck & Page (1997), who find that, for  $\lambda < 1/3$ , a steady state does indeed develop, but for larger values of  $\lambda$ , a finite-time singularity arises in the boundary layer, consistent with what we find in §4 for the oscillatory case, where we also find the possibility of finite-time singularities near the rear stagnation point when the cylinder is accelerated to its long-time state.

Finally, as we have implied above and will become explicit in the next Section, throughout the analysis the Rossby number,  $\epsilon$ , is  $O(E^{1/2})$ . Typical numbers for an oceanic seamount, say the Fieberling Guyot, as quoted in Boyer *et al.* (1991), give the ratio  $\epsilon/E^{1/2} = U/(v\Omega)^{1/2}$  to be no smaller than 10 at best, so the direct applicability of this analysis is weak, except for the fact that the proper choice of  $v$  for turbulent transport is not really known, and a factor of 3 or so larger than the number taken by Boyer ( $0.1 \text{ m}^2 \text{ s}^{-1}$ ) puts such a seamount into the parameter range of this paper. For the most part, this analysis ought to be thought of as a limiting case. It is worth pointing out that the ratio  $\epsilon/E^{1/2}$ , being independent of any length scale, depends on two variable quantities only:  $v$  and  $U$ .

## 2. Problem formulation

We consider now the flow of an incompressible fluid between two infinite parallel plates, located at  $z' = 0$  and  $z' = h$ , with a right circular cylinder with diameter  $2ah$  and height less than or equal to  $h$ , standing at the origin (figure 1). The plates and cylinder rotate about the  $z'$ -axis with angular velocity  $\Omega$ . The coordinate system rotates with the plates and cylinder. A uniform oscillating flow of speed  $U(1 + \gamma \cos(\omega't))$  is forced between the plates in the positive  $x'$ -direction. The flow is characterized by a number of dimensionless parameters, which are the Ekman number  $E$ , Rossby number  $\epsilon$ , oscillation amplitude  $\gamma$ , and oscillation frequency  $\omega$ , with  $E$ ,  $\epsilon$ , and  $\omega$  defined respectively by

$$E \equiv \frac{\nu}{\Omega h^2}, \quad \epsilon \equiv \frac{U}{\Omega h}, \quad \omega \equiv \frac{\omega'}{\Omega E^{1/2}}. \quad (2.1)$$

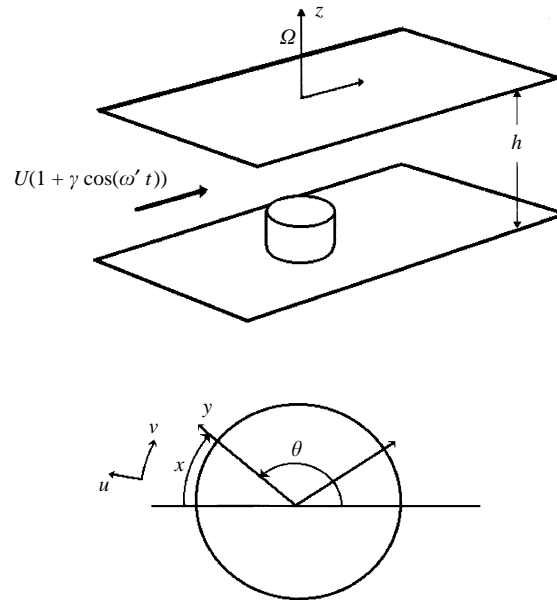


FIGURE 1. Geometric configuration for the problem under study. The labels  $(x, y)$  and  $(u, v)$  indicate the notation used in the boundary-layer analysis.

The non-dimensional equations of motion for this problem are

$$\nabla \cdot \mathbf{u} = 0, \quad (2.2)$$

$$E^{1/2} \frac{\partial \mathbf{u}}{\partial t} + \epsilon (\mathbf{u} \cdot \nabla) \mathbf{u} + 2\mathbf{k} \times \mathbf{u} + \nabla p = E \nabla^2 \mathbf{u}. \quad (2.3)$$

$$\mathbf{u} = \mathbf{0} \quad \text{on solid surfaces}, \quad (2.4)$$

$$\mathbf{u} \sim (1 + \gamma \cos(\omega t)) \nabla x \quad \text{for } |\mathbf{x}| \rightarrow \infty, \quad (2.5)$$

where lengths have been made dimensionless with  $h$ , velocities with  $U$ , pressure by  $\rho U \Omega h$ , frequency by  $\Omega E^{1/2}$ , as noted above, and time by a compatible scaling  $(\Omega E^{1/2})^{-1}$ . This choice of time scale makes the quarter layer fully unsteady. For shorter time scales (and higher frequencies), the layer structure is quite different, involving a Stokes layer, for example; on longer time scales, the quarter layer is essentially steady, so there are no unsteady effects in boundary-layer breakaway.

The analysis of the geostrophic flow past a circular cylinder, obtained by letting  $\epsilon$  and  $E$  go to zero in the equations of motion and incorporating the effects of Ekman suction on the walls, is well known; see, for example, Foster (1972). The result is that the outer flow is essentially the classical solution for irrotational incompressible flow past a circular cylinder (cf. Barcilon 1970), in this case with an oscillatory free stream,

$$\mathbf{u}_o = (1 + \gamma \cos(\omega t)) \nabla \left( (1 + a^2/r^2) r \cos(\theta) \right). \quad (2.6)$$

The Taylor–Proudman theorem implies, of course, that this geostrophic flow is independent of the vertical coordinate,  $z$ . In contrast with the classical problem of flow past a cylinder, the presence of the Coriolis forces in the boundary layer delays onset of boundary-layer separation to quite high Reynolds numbers, as we know from Walker & Stewartson (1972), as discussed in §1. So, we turn to the solution of the boundary-layer equation on the cylindrical surface.

The structure of the Stewartson layers on the cylindrical surface may be found throughout the rotating-flow literature (again, see Foster 1972, as an example), so we omit all details here and simply note that since the 1/3-layer is passive, and quasi-steady on this time scale, all of the dynamics occurs in the layer of width  $E^{1/4}$ , referred to throughout this paper as the ‘quarter layer’. Because of the circular geometry, we begin with the usual circular polar coordinates  $(r, \theta, z)$ . Since the flow is left-to-right (see figure 1), the rear stagnation point is at  $\theta = 0$ , so it is better to use intrinsic coordinates with origin at the forward stagnation point. Thus, we write the radial and  $\theta$  velocity components as  $E^{1/4}u/a$  and  $-v$  respectively, and define a coordinate along the surface,  $x \equiv \pi - \theta$ . Then, the limit of the equations of motion (2.2), (2.3) as  $E \rightarrow 0$  for  $y \equiv (r - a)/E^{1/4}$  fixed is

$$\frac{\partial v}{\partial x} + \frac{\partial u}{\partial y} = 0, \quad (2.7)$$

$$\frac{\partial v}{\partial t} + \lambda \left( v \frac{\partial v}{\partial x} + u \frac{\partial v}{\partial y} \right) + 2v = \frac{\partial v_e}{\partial t} + \lambda v_e \frac{\partial v_e}{\partial x} + 2v_e + \frac{\partial^2 v}{\partial y^2}. \quad (2.8)$$

In these equations,  $v_e$  is the  $\theta$ -direction velocity at the edge of the layer, obtained from (2.6):

$$v_e = 2 \sin(x) (1 + \gamma \cos(\omega t)). \quad (2.9)$$

The parameter in (2.8) which measures the importance of fluid inertia is

$$\lambda \equiv \frac{\epsilon}{E^{1/2}a}. \quad (2.10)$$

We note that (2.7), (2.8) are precisely the equations for the Prandtl boundary layer on the surface of the cylinder apart from the very significant addition of the Coriolis term. So, to complete the specification of the problem, we note that the boundary conditions are

$$u(x, 0, t) = 0, \quad v(x, 0, t) = 0, \quad v(x, \infty, t) = v_e, \quad (2.11)$$

$$v(0, y, t) = 0, \quad v(\pi, y, t) = 0. \quad (2.12)$$

Boundary condition (2.12) needs further explanation. Because the problem domain is about a cylinder, the velocities are periodic in  $x$ , which is a single boundary condition connecting two distinct boundaries. Furthermore, when we cut the domain in half by symmetry, we still need to say something about both boundaries. Since  $v$  is an odd function of  $x$ , conditions (2.12) follow; it is a single boundary condition, even though it looks like two.

In previous discussions of the steady problem (Page & Cowley 1988; Page 1985; Walker & Stewartson 1972), an ‘interaction parameter’  $N$  was used to characterize the nonlinearity, instead of our quantity  $\lambda$ , in order to maintain the connection with the equivalent magnetohydrodynamic problem, which is governed by the same equations (Buckmaster 1971, 1969; Leibovich 1967). This paper uses  $\lambda$ , and these two parameters are related by

$$N = \frac{1}{\lambda}. \quad (2.13)$$

The solution of equations (2.7), (2.8), subject to (2.11), (2.12), occupies the rest of this paper. There are two other parameters of note in the equations:  $\gamma$  and  $\omega$ . In the next Section, we explore a number of analytical and asymptotic solutions for small values of  $\lambda$  and/or  $1/\omega$  before turning to the more general problem when these parameters are of  $O(1)$ .

### 3. Analytic and asymptotic results

With three parameters in them, the quarter-layer equations (2.7), (2.8) yield readily to asymptotic analysis. There are also several analytical results that are valid without taking an asymptotic limit. We consider first under what circumstances the assumed edge velocity (2.8) can be shown to be consistent with an initial-value problem for the quarter layer. Next, we find an asymptotic solution in the  $\lambda \rightarrow 0$  limit. Finally, we consider the  $\omega \rightarrow \infty$  limit, with  $\lambda, \gamma = O(1)$ . A few other asymptotic cases, and more detail of what follows may be found in Kunka (1991).

#### 3.1. Stability of the edge velocity

In the formulation of this problem, we have taken the edge velocity to be given by (2.9). The question is as follows: Is the edge condition consistent with a general initial-value problem for this flow? We can determine the  $\lambda$ -range for which a solution is in the form we seek by examining the stability of the equations at the edge of the quarter layer, to see if the edge velocity is a stable solution there. For simplicity, we consider only the linear stability problem.

We begin by assuming that the velocity  $v$  in the quarter layer consists of the steady solution plus a small perturbation, then take the limit of (2.8) as  $y \rightarrow \infty$ ,

$$v = v_e + \delta v_e(x, t), \tag{3.1}$$

$$\frac{\partial}{\partial t} \delta v_e + \lambda v_e \frac{\partial}{\partial x} (\delta v_e) + \left( 2 + \lambda \frac{\partial v_e}{\partial x} \right) (\delta v_e) = 0, \tag{3.2}$$

where we have neglected small nonlinear terms to obtain (3.2) and further supposed that viscous terms are small at the edge. The solution of equation (3.2) is easily found to be

$$\left. \begin{aligned} \delta v_e(x, t) &= \frac{\delta v_{e0}(x_0) e^{-2t}}{\cosh(q(t)) + \sinh(q(t)) \cos(x)}, \\ q(t) &\equiv 2\lambda \left( t + \frac{\gamma}{\omega} \sin(\omega t) \right), \end{aligned} \right\} \tag{3.3}$$

where  $x_0$  is the value of  $x$  where the characteristic leaves the  $t = 0$  line, and  $\delta v_{e0}(x)$  is the initial value of the perturbation. The quantity  $x_0$  is given implicitly by the equation

$$\tan \left( \frac{1}{2} x_0 \right) = \tan \left( \frac{1}{2} x \right) e^{-2\lambda(t + (\gamma/\omega) \sin(\omega t))}. \tag{3.4}$$

It is immediately evident from the long-time behaviour of (3.3) that the disturbance decays for all positive values of  $\lambda$ ,

$$\delta v_e(x, t) \sim \frac{\delta v_e(x_0) 2e^{-2(1+\lambda)t - (2\lambda\gamma/\omega) \sin(\omega t)}}{1 + \cos(x)} \quad \text{for } t \rightarrow \infty, x < \pi. \tag{3.5}$$

However, this solution is not the proper long-time limit of (3.3) near  $x = \pi$ . Precisely at  $x = \pi$ , (3.3) gives

$$\delta v_e \sim \delta v_{e0}(\pi) e^{-2(1-\lambda)t + (2\lambda\gamma/\omega) \sin(\omega t)} \quad \text{for } t \rightarrow \infty, \tag{3.6}$$

so there is clearly some difficulty near the rear stagnation point, since this perturbation decays to zero only so long as  $\lambda$  is less than 1. We explore in much greater detail the behaviour of the solutions near  $x = \pi$  in §4. Finally, a look at the characteristic map from (3.4) shows that all characteristics leaving the  $t = 0$  line eventually asymptote  $x = \pi$ , except the one from  $x = 0$ . Thus the forward stagnation point similarity solution makes sense at long times, but again there is obvious trouble near  $x = \pi$ .

3.2. Weakly nonlinear case:  $\lambda \ll 1$ 

In this case, the long-time leading-order solution is just a generalization of the linear solution of Barcion (1970) and Walker & Stewartson (1972). The oscillatory free stream has an order-one effect on the leading-order flow. This case thus provides an excellent test for verifying the numerical method used in §5.

The solution is written as a regular perturbation expansion, with velocity components expanded in asymptotic series that begin

$$v = v_0 + \lambda v_1 + \dots, \quad u = u_0 + \lambda u_1 + \dots \quad (3.7)$$

The higher-order corrections to the outer flow require  $\lambda \gg E^{1/4}$  for the series to be of the form (3.7). These series are substituted into the governing equations (2.7), (2.8) and like powers of  $\lambda$  are collected and each problem for  $v_i$  and  $u_i$  is solved in turn, in the usual way. The linear equations are solved with the help of Laplace transforms and only that part of the Laplace inversion corresponding to the long-time periodic solution is given here; transients are not written down. Hence, the leading-order solution for  $t \rightarrow \infty$  is

$$v_0 = 2 \sin(x) \left(1 - e^{-\sqrt{2}y}\right) + 2\gamma \sin(x) [\cos(\omega t) - e^{-Ay} \cos(\omega t - By)], \quad (3.8)$$

$$\begin{aligned} rlu_0 = & -2 \cos(x) \left[ y - \frac{1}{\sqrt{2}} \left(1 - e^{-\sqrt{2}y}\right) \right] \\ & - 2\gamma \cos(x) \left[ y \cos(\omega t) + \frac{e^{-Ay}}{A^2 + B^2} (A \cos(\omega t - By) + B \sin(\omega t - By)) \right] \\ & + 2\gamma \frac{\cos(x)}{A^2 + B^2} (A \cos(\omega t) + B \sin(\omega t)), \end{aligned} \quad (3.9)$$

where

$$A = \operatorname{Re}((2 + i\omega)^{1/2}) = \left(\frac{1}{2}(4 + \omega^2)^{1/2} + 1\right)^{1/2}, \quad (3.10a)$$

$$B = \operatorname{Im}((2 + i\omega)^{1/2}) = \left(\frac{1}{2}(4 + \omega^2)^{1/2} - 1\right)^{1/2}. \quad (3.10b)$$

Clearly, if  $\lambda \equiv 0$ , then (3.8), (3.9) is the exact solution for all  $\gamma$  and  $\omega$ . The details of the first correction  $v_1$  can be found in Kunka (1991), and are summarized in the Appendix.

Using the solution for  $v_0$ , the leading-order shear stress and displacement thickness are found to be

$$\tau_{wall} = \left. \frac{\partial v_0}{\partial y} \right|_{y=0} = 2 \sin(x) \left[ \sqrt{2} + \gamma(A \cos(\omega t) - B \sin(\omega t)) \right], \quad (3.11)$$

$$\delta_0^* = \int_0^\infty \left(1 - \frac{v_0}{v_e}\right) dy = \frac{1/\sqrt{2} + [\gamma/(A^2 + B^2)](A \cos(\omega t) + B \sin(\omega t))}{1 + \gamma \cos(\omega t)}. \quad (3.12)$$

An examination of (3.11) reveals that, for a given  $\omega$ , if  $\gamma$  is large enough, and still less than one, the shear stress will periodically become negative, namely the flow will periodically reverse.

3.3. High-frequency oscillation:  $\omega \gg 1, \lambda = O(1)$ 

We consider now the character of the quarter-layer solution for high oscillation frequency, and to that end define a scaled time variable,  $\tau \equiv \omega t$ , and take  $\tau = O(1)$



with  $\omega \gg 1$ . Substitution of this change of variable into (2.8) leads to a scaled quarter-layer equation,

$$\frac{\partial v}{\partial \tau} - \frac{\partial v_e}{\partial \tau} + \frac{\lambda}{\omega} \left[ u \frac{\partial v}{\partial y} + v \frac{\partial v}{\partial x} - v_e \frac{\partial v_e}{\partial x} \right] + \frac{2}{\omega} (v - v_e) = \frac{1}{\omega} \frac{\partial^2 v}{\partial y^2}. \quad (3.13)$$

We write the outer expansion as

$$v = v_0 + \frac{1}{\omega} v_1 + \dots, \quad \lambda = O(1). \quad (3.14)$$

and substitution of (3.14) into (3.13) leads to a hierarchy of perturbation problems, the first of which is

$$\frac{\partial v_0}{\partial \tau} - \frac{\partial v_e}{\partial \tau} = 0, \quad (3.15)$$

whose solution is

$$v_0 = v_e + F(x, y). \quad (3.16)$$

Working to next order leads to the equation for  $v_1$ ,

$$\frac{\partial v_1}{\partial \tau} = \frac{\partial^2 F}{\partial y^2} - 2F - \lambda \left[ (-y v_{ex} + \hat{u}_0) \frac{\partial F}{\partial y} + \frac{\partial}{\partial x} (v_e F + \frac{1}{2} F^2) \right], \quad (3.17)$$

$$\frac{\partial \hat{u}_0}{\partial y} + \frac{\partial F}{\partial x} = 0, \quad u_0 = -y v_{ex} + \hat{u}_0. \quad (3.18)$$

Terms on the right-hand side of (3.17) that are time-periodic lead to periodic portions of  $v_1$ ; those terms that are time-independent lead to secular terms in  $v_1$ , invalidating the asymptotic series (3.14) at long times. Thus, to avoid that secularity, we require that all time-independent terms on the right-hand side of (3.17) add up to zero. Hence,

$$\frac{\partial^2 F}{\partial y^2} - 2F - \lambda \left[ (-y v_{ex}^{(s)} + \hat{u}_0) \frac{\partial F}{\partial y} + \frac{\partial}{\partial x} (v_e^{(s)} F + \frac{1}{2} F^2) \right] = 0, \quad (3.19)$$

where we have split the edge velocity,  $v_e$ , into time-independent and time-periodic components, as

$$\left. \begin{aligned} v_e &= v_e^{(s)} + v_e^{(p)}, \\ v_e^{(s)} &= 2 \sin(x), \quad v_e^{(p)} = 2\gamma \sin(x) \cos \tau. \end{aligned} \right\} \quad (3.20)$$

For convenience, then, we also let  $V_0(x, y)$  denote the time-independent portion of  $v_0$ , so therefore,

$$\left. \begin{aligned} v_0 &= v_e + F = (v_e^{(s)} + F) + v_e^{(p)} = V_0 + v_e^{(p)}, \\ \hat{u}_0 &= U_0 + y v_{ex}^{(s)}. \end{aligned} \right\} \quad (3.21)$$

Hence, in this notation, equation (3.19) becomes

$$\left. \begin{aligned} \frac{\partial^2 V_0}{\partial y^2} - 2(V_0 - v_e^{(s)}) - \lambda \left[ U_0 \frac{\partial V_0}{\partial y} + V_{\frac{\partial v_0}{\partial x}} - v_e^{(s)} \frac{d v_e^{(s)}}{dx} \right] &= 0, \\ \frac{\partial U_0}{\partial y} + \frac{\partial V_0}{\partial x} &= 0. \end{aligned} \right\} \quad (3.22)$$

Therefore,  $(U_0, V_0)$  satisfy precisely the quarter-layer equations for the steady flow past the cylinder – on this outer- $y$  scale. Having avoided secular terms in  $v_1$ , equation

(3.17) now reduces to a simpler form,

$$\frac{\partial v_1}{\partial \tau} = -\lambda \left[ \frac{\partial v_e^{(p)}}{\partial x} \left( F - y \frac{\partial F}{\partial y} \right) + v_e^{(p)} \frac{\partial F}{\partial x} \right], \quad (3.23)$$

so integrating, we obtain the simple result

$$v_1 = -2\lambda\gamma \sin \tau \left[ \cos(x) \left( F - y \frac{\partial F}{\partial y} \right) + \sin(x) \frac{\partial F}{\partial x} \right] + G(x, y), \quad (3.24)$$

where  $G(x, y)$  is determined by eliminating secular terms in the next order. In order to match to the lower layer, we need to evaluate the outer expansion for small  $y$ . Hence, using these solutions, we have the behaviour of  $v$  for small  $y$ ,

$$v \sim v_e^{(p)} + V_{0y}(x, 0)y + \frac{1}{2}y^2 V_{0yy}(x, 0) + \dots + \frac{1}{\omega} v_1(x, 0) + \dots \quad (3.25)$$

Examination of the equation (3.13) indicates that the appropriate inner limit gives a Stokes layer, so  $y = Y/\omega^{1/2}$ , and hence the form of (3.25) suggests an inner expansion in the form

$$v \sim \tilde{v}_0(x, Y, \tau) + \omega^{-1/2} \tilde{v}_1(x, Y, \tau) + \omega^{-1} \tilde{v}_2(x, Y, \tau) + \dots \quad (3.26)$$

The limit of (3.13) for  $Y$  fixed and  $\omega \rightarrow \infty$  is

$$\frac{\partial \tilde{v}_0}{\partial \tau} - \frac{\partial v_e^{(p)}}{\partial \tau} = \frac{\partial^2 \tilde{v}_0}{\partial Y^2}. \quad (3.27)$$

The solution which matches to the first term of (3.25) is

$$\tilde{v}_0 = 2\gamma \left[ \cos \tau - e^{-Y/\sqrt{2}} \cos(\tau - Y/\sqrt{2}) \right] \sin(x). \quad (3.28)$$

The second term in (3.26) satisfies an equation like (3.27) but without the  $v_e$  term, and its solution, which matches to the second term in (3.25), is  $v_1 = V_{0y}(x, 0)Y$ . The  $v_2$  equation may be put in the form

$$\frac{\partial \tilde{v}_2}{\partial \tau} + \lambda \left[ \tilde{u}_0 \frac{\partial \tilde{v}_0}{\partial Y} + \tilde{v}_0 \frac{\partial \tilde{v}_0}{\partial x} - v_e \frac{\partial v_e}{\partial x} \right] + 2(\tilde{v}_0 - v_e) = \frac{\partial^2 \tilde{v}_2}{\partial Y^2}, \quad (3.29)$$

which, according to (3.25), must have the large- $Y$  behaviour given by

$$\tilde{v}_2 \sim -Y^2 \left[ v_e^{(s)} + \frac{1}{2} \lambda v_e^{(s)} \frac{dv_e^{(s)}}{dx} \right] + 4\lambda\gamma \sin(2x) \sin \tau \quad \text{for } Y \rightarrow \infty. \quad (3.30)$$

It is simplest to construct the solution to (3.29) by writing it as follows:

$$\tilde{v}_2 = -Y^2 \left[ v_e^{(s)} + \frac{1}{2} \lambda v_e^{(s)} \frac{dv_e^{(s)}}{dx} \right] + 4\lambda\gamma \sin(2x) \sin \tau + \dot{v}_2, \quad (3.31)$$

in which case equation (3.29) reduces to the simpler form

$$\left. \begin{aligned} \frac{\partial \dot{v}_2}{\partial \tau} + \lambda \left[ \dot{u}_0 \frac{\partial \dot{v}_0}{\partial Y} + \dot{v}_0 \frac{\partial \dot{v}_0}{\partial x} \right] - \lambda \frac{\partial v_e^{(p)}}{\partial x} \left( Y \frac{\partial \dot{v}_0}{\partial Y} - \dot{v}_0 \right) &= \frac{\partial^2 \dot{v}_2}{\partial Y^2}, \\ \tilde{v}_0 = v_e^{(p)} + \dot{v}_0, \quad \tilde{u}_0 = -Y \frac{\partial v_e^{(p)}}{\partial x} + \dot{u}_0. \end{aligned} \right\} \quad (3.32)$$

It is evident from the form of (3.31) and (3.32) that the solution satisfies the matching condition given by (3.30). The solution for  $\dot{v}_2$  is a complicated exercise and is not included here only because the result is not particularly instructive.

There are several important features of this high-frequency approximation. First, the solution outside the Stokes layer is dominated by the steady solution, so all of the singularity structure derived by Page & Cowley (1988) immediately applies. This means that the high-frequency solution exists for  $\lambda < 1$  and does not for  $\lambda > 1$ . Second, it means that our ability to obtain solutions to the complete unsteady problem will depend, at least indirectly, on our ability to solve the steady problem. Third, since all of the non-trivial unsteady behaviour is restricted to a Stokes layer of thickness  $O(\omega^{-1/2})$ , the wall region must be adequately resolved to obtain numerical solutions to the unsteady equations for large numerical values of  $\omega$ . We use this information to our advantage when obtaining the numerical solutions in §5.

#### 4. Similarity solution at the rear stagnation point

The rear stagnation point is perhaps the most interesting and certainly the most critical region of the flow. Much of the early work on the steady magnetohydrodynamic version of this problem (Buckmaster 1971, 1969; Leibovich 1967) focused on this region, initially with the similarity form of the governing equations and their solutions. It is well known that they verified that a steady similarity solution satisfying the correct boundary conditions exists if  $\lambda < 1/2$ . It is also known that, for  $1/2 < \lambda < 1$ , a similarity solution can be found if the correct edge velocity is replaced by a ‘plateau’ velocity, indicating that a singularity exists at the rear stagnation point in this  $\lambda$ -range, but Buckmaster (1971, 1969) and Leibovich (1967) were unable to determine an outer-layer structure that would bridge the gap between the plateau velocity and the edge velocity – a task which went uncompleted until Page & Cowley (1988). Here, we extend the analysis of the self-similar solution to the oscillatory case. We begin by deriving the unsteady similarity equations, and then investigate the stability of the edge boundary condition, as we did in §3.1. A large- $y$  expansion of the solution verifies that the appropriate edge conditions can indeed be satisfied in a self-consistent way. Finally, we solve the similarity equations numerically, to verify that a solution exists.

##### 4.1. The unsteady similarity equations

The general self-similar equation is derived in the standard way. The velocities are written in terms of a stream function,  $f$ , with the  $x$ -dependence factored out, so we have

$$\left. \begin{aligned} v_e &\sim 2(\pi - x)(1 + \gamma \cos(\omega t)), \\ v &\sim 2(\pi - x)f_y(y, t), \quad u \sim 2f(y, t), \quad |\pi - x| \ll 1. \end{aligned} \right\} \quad (4.1)$$

These solutions do of course represent leading-order terms in an asymptotic series in odd powers of  $(\pi - x)$ . Substitution of (4.1) into (2.7)–(2.9) produces the similarity equation and boundary conditions governing the flow near the rear stagnation point,

$$\bar{v}_t + \gamma\omega \sin(\omega t) + 2\lambda [f \bar{v}_y - \bar{v}^2 + (1 + \gamma \cos(\omega t))^2] + 2(\bar{v} - (1 + \gamma \cos(\omega t))) = \bar{v}_{yy}, \quad (4.2)$$

$$\bar{v} \equiv f_y, \quad (4.3)$$

$$f(0, t) = \bar{v}(0, t) = 0, \quad (4.4)$$

$$\bar{v}(\infty, t) = 1 + \gamma \cos(\omega t). \quad (4.5)$$

## 4.2. Stability of the edge velocity

We know that for the  $\gamma = 0$  case the edge boundary condition (4.5) is not valid for all  $\lambda$ . The same is true for the  $\gamma \neq 0$  situation. We can determine the range of  $\lambda$  for which (4.5) is valid by testing the stability of the equations as  $y \rightarrow \infty$ . Assuming that the velocity has a limiting value  $\bar{v}_e$  as  $y$  increases to infinity, the governing equation (4.2) becomes

$$\frac{d\bar{v}_e}{dt} + \gamma\omega \sin(\omega t) + 2\lambda \left( (1 + \gamma \cos(\omega t))^2 - \bar{v}_e^2 \right) + 2(\bar{v}_e - (1 + \gamma \cos(\omega t))) = 0. \quad (4.6)$$

We now suppose that the edge velocity  $\bar{v}_e$  consists of the sum of the specified edge velocity (4.5) and a time-dependent perturbation, which is not taken to be small. Substitution into (4.6) gives the governing equation for the perturbation  $\delta v_e$ :

$$\bar{v}_e = 1 + \gamma \cos(\omega t) + \delta v_e(t), \quad (4.7)$$

$$\frac{d}{dt}(\delta v_e) + 2(1 - 2\lambda(1 + \gamma \cos(\omega t))) \delta v_e = 2\lambda(\delta v_e)^2. \quad (4.8)$$

Equation (4.8) is a Bernoulli equation, so, with a bit of effort, its exact solution can be found. Thus, the time-dependent edge velocity for any initial condition  $\delta v_e(0)$  is given by

$$\bar{v}_e(t) = 1 + \gamma \cos(\omega t) + \frac{\delta v_e(0) e^{-2(1-2\lambda)t+4(\lambda\gamma/\omega) \sin(\omega t)}}{1 - \delta v_e(0) 2\lambda [e^{-2(1-2\lambda)t} F(t) - F(0)]}, \quad (4.9)$$

where

$$F(t) = \frac{I_0(z)}{2(2\lambda - 1)} + S_1(t) + S_2(t), \quad (4.10)$$

$$S_1(t) = 2 \sum_{k=0}^{\infty} \frac{(-1)^k I_{2k+1}(z)}{(2k+1)^2 \omega^2 + 4(2\lambda - 1)^2} \times [2(2\lambda - 1) \sin((2k+1)\omega t) - (2k+1)\omega \cos((2k+1)\omega t)], \quad (4.11)$$

and

$$S_2(t) = 2 \sum_{k=1}^{\infty} \frac{(-1)^k I_{2k}(z)}{4k^2 \omega^2 + 4(2\lambda - 1)^2} [2(2\lambda - 1) \cos(2k\omega t) + 2k\omega \sin(2k\omega t)]. \quad (4.12)$$

The parameter  $z$  is  $4\lambda\gamma/\omega$  and  $I_n(z)$  is the modified Bessel function of first kind. The solution (4.9)–(4.12) has a number of interesting features. Most important, the solution for  $F$  is periodic, of period  $2\pi/\omega$ . If  $z$  is small, the Fourier coefficients decay like  $z^n/n$  ( $n = 2k$  or  $2k+1$ ), i.e. only the first few harmonics are appreciable. On the other hand, if  $z$  is large, the Bessel functions are independent of  $n$  at leading order, so the Fourier coefficients are all important, and many frequencies are a part of the solution.

The long-time behaviour of (4.9) depends on  $\lambda$ . If  $\lambda < 1/2$ , then the exponentials are decaying, and the long-time solution is the edge velocity (4.5). If  $\lambda > 1/2$ , however, the exponentials are increasing and the long-time solution becomes the plateau velocity

$$\bar{v}_p(t) = 1 + \gamma \cos(\omega t) - \frac{1}{2\lambda} \frac{e^{4(\lambda\gamma/\omega) \sin(\omega t)}}{F(t)}. \quad (4.13)$$

Therefore, the critical value of  $\lambda$  that separates the stable ‘edge velocity’ (4.5) from the stable ‘plateau velocity’ (4.13) is  $\lambda = 1/2$ , independent of  $\gamma$  and  $\omega$ . Also, nothing

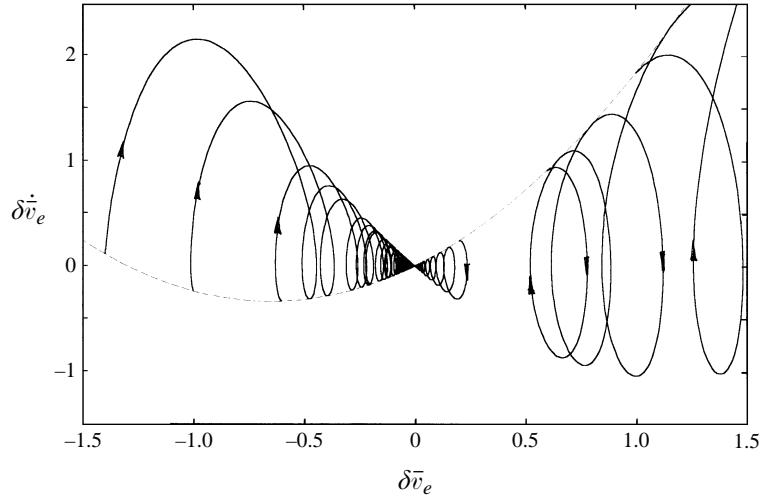


FIGURE 2. Phase trajectories for  $\delta \bar{v}_e$ ;  $\lambda = 0.40$ ,  $\omega = 2\pi$  and  $\gamma = 0.90$  for several different initial values. The dashed parabolic curve is the locus of initial conditions.

special occurs if  $\lambda > 1$ , indicating that the above analysis is unable to determine when no solution exists. (Remember that we assumed that the velocity is finite at infinity in deriving (4.6).)

However, the most general initial-value problem for this flow, and for the edge velocity in particular, indicates that, in fact, a singularity in the edge velocity may develop at finite times. It is not the primary purpose of this paper to establish the character of a general initial-value problem for the flow at hand. Notice, however, that there is much to be learned in this regard from (4.9). In particular, for values of  $\lambda < 1/2$ , (4.9) shows that if the initial perturbation  $\delta v_e(0)$  is sufficiently small, then the second term in the denominator of (4.9) is small uniformly in time, and hence the perturbation  $\delta v_e$  vanishes for long times and there is no possibility that the denominator might vanish (figure 2). Similarly, if  $\lambda > 1/2$  and the initial perturbation from the edge velocity is such that the velocity is near enough to the (stable) plateau velocity, then, once again, the perturbation decays at long time and no finite singularity develops (figure 3). From figures 2 and 3, a finite-time singularity will only occur for a sufficiently large initial perturbation from the edge velocity (which is stable for  $\lambda < 1/2$ ) or the plateau velocity (which is stable for  $\lambda > 1/2$ ). The finite-time singularity occurs when the denominator in (4.9) goes to zero, say at a time  $t_s$ , provided that the initial condition satisfies the constraint

$$\delta v_e(0) = \frac{1}{2\lambda(e^{2(2\lambda-1)t_s}F(t_s) - F(0))} \quad \text{for some } t_s > 0. \quad (4.14)$$

For cases when there is such a breakdown, equation (4.8) indicates that the solution takes the form

$$\delta v_e \sim \frac{1}{2\lambda(t_s - t)} + \frac{1 - 2\lambda(1 + \gamma \cos(\omega t_s))}{2\lambda} + \dots \quad \text{for } t \rightarrow t_s. \quad (4.15)$$

To deal more completely with this question, solutions for equation (4.8) may easily be obtained numerically. The results are shown as phase trajectories in figures 2 and 3. (The dashed line in the figures is the locus of possible initial values, since the system is first order.) In figure 2, for a value of  $\lambda = 0.40$ , the phase trajectories of the

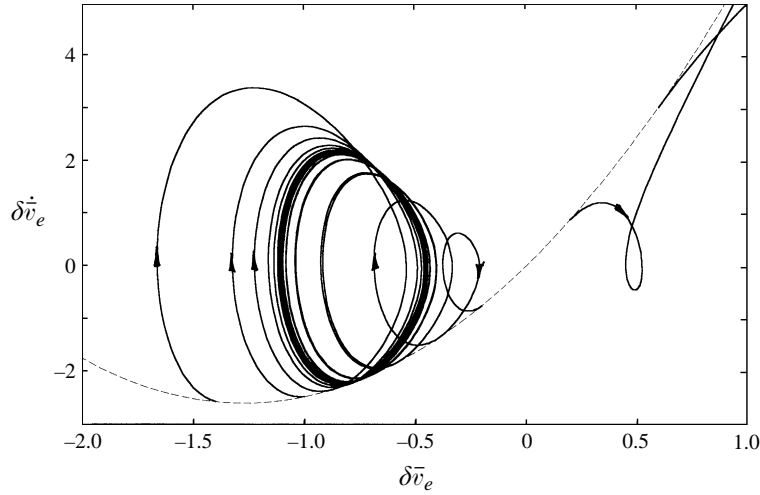


FIGURE 3. Phase trajectories for  $\delta \bar{v}_e$ ;  $\lambda = 0.80$ ,  $\omega = 2\pi$  and  $\gamma = 0.90$  for several different initial values. The dashed parabolic curve is the locus of initial conditions.

solutions show that, regardless of the choice of  $\delta v_e(0)$  near the origin, all solutions approach the origin as  $t \rightarrow \infty$ , validating the use of (4.5) for values of  $\lambda$  less than  $1/2$ . Furthermore, the plateau velocity is unstable for this  $\lambda$  and so a large enough  $\delta v_e(0)$  ( $> 1.5$  for example) will cause the finite time singularity to occur. On the other hand, since  $\bar{v}_e$  is between 0 and 2 for various values of  $t$  with  $\gamma < 1$ , such a large initial disturbance seems unlikely.

The situation changes somewhat as  $\lambda$  approaches  $1/2$ . In this case, the plateau and edge velocities almost coincide, so that even small (non-infinitesimal) positive  $\delta v_e$  will cause the finite-time singularity to occur.

For  $\lambda = 0.80$  ( $> 1/2$ ), figure 3 indicates that if the initial velocity is near the plateau, then the finite-time singularity is avoided. On the other hand, if the initial condition is near the (unstable) edge velocity, then the finite-time singularity occurs whenever  $\delta v_e(0) > 0$ .

We conclude, then, as implied by (4.14), that for  $\delta v_e(0)$  sufficiently large, the rear-stagnation-point similarity solution develops a singularity in finite time. Such singularities may be rare since they require large initial deviations from the edge velocity (for  $\lambda < 1/2$ ) or the plateau velocity (for  $\lambda > 1/2$ ), but the singularity may be more common for  $\lambda \sim 1/2$ . For  $\lambda > 1/2$ , if the initial value for  $\bar{v}_e$  is near the edge velocity, (4.5), then the appearance of the singularity is more likely.

We proceed in what follows on the assumption that the initial conditions for the flow are such that (4.5) and (4.13) are indeed the long-time solutions for the edge velocity. We now further explore the near-edge structure implied by the requirement that  $v$  has a finite limit as  $y \rightarrow \infty$ .

Further discussion of the possibilities of finite-time appearance of singularities near the rear stagnation point may be found in Stocker *et al.* (1997). As noted earlier, in exploring the startup of a cylinder from rest, they find that indeed a finite-time singularity does appear near the rear stagnation point for  $\lambda > 1/3$ , whereas our work shows evidence for that occurrence for all values of  $\lambda > 1/2$ . For values below  $\lambda = 1/2$ , our discussion above is not conclusive. What we do show is that even in  $\lambda > 1/2$ , a decelerating flow seems to be stable.

4.3. Large- $y$  asymptotic solution

In order to show that a solution exists which satisfies the edge velocity (4.5) for  $\lambda < 1/2$  and the plateau velocity (4.13) for  $1/2 < \lambda < 1$ , we rewrite the velocities as perturbations about the appropriate edge condition and derive the equation for the perturbations:

$$f = y\bar{v}_e(t) + \Phi(y, t), \quad \bar{v} = \bar{v}_e(t) + \Phi_y(y, t) = \bar{v}_e(t) + \phi(y, t). \quad (4.16)$$

The question is, does  $\Phi/y$  go to zero for  $y \rightarrow \infty$ ? We begin by assuming an algebraic behaviour in  $y$ ; then, from (4.16),

$$\Phi \sim y^{\alpha+1}A(y, t), \quad \phi \sim y^\alpha ((\alpha + 1)A + yA_y) = y^\alpha B(y, t), \quad (4.17)$$

$$B_t + 2\lambda\bar{v}_e(t)yB_y + 2(1 - \lambda(\alpha - 2)\bar{v}_e(t))B = 0. \quad (4.18)$$

We require that  $A$  and  $B$  are non-zero and finite as  $y, t \rightarrow \infty$ , so that (4.17) are in fact the leading-order contributions. Clearly,  $\alpha < 0$  is required for the perturbation  $\phi$  to decay at infinity. Equation (4.18) is readily solved; the solution is

$$B(y, t) = B_0 \left( y \exp \left[ -2\lambda \int_0^t \bar{v}_e(\tau) d\tau \right] \right) \exp \left[ -2t - 2\lambda(\alpha - 2) \int_0^t \bar{v}_e(\tau) d\tau \right]. \quad (4.19)$$

The function  $B_0(y)$  is determined, in principle, by matching to the  $O(1)$  part of the boundary layer at  $t = 0$ .

We now consider the case  $0 < \lambda < 1/2$ . The edge velocity is (4.5) and the integrals in (4.19) are easily evaluated:

$$B(y, t) = B_0 \left( y e^{-2\lambda(t+(\gamma/\omega)\sin(\omega t))} \right) e^{-2(1+\lambda(\alpha-2))t-2(\lambda\gamma/\omega)\sin(\omega t)}. \quad (4.20)$$

The requirement that  $B(y, t)$  be non-zero and finite as  $t \rightarrow \infty$  requires that

$$1 + \lambda(\alpha - 2) = 0. \quad (4.21)$$

or

$$\alpha = 2 - 1/\lambda, \quad (4.22)$$

which is less than zero for  $0 < \lambda < 1/2$ . This exponent is independent of  $\gamma$  and  $\omega$  and agrees with the steady results of Buckmaster (1969) and Leibovich (1967).

For  $1/2 < \lambda < 1$ , it would still seem to be the case that boundedness for  $B$  as  $t \rightarrow \infty$  leads to a requirement from (4.19) that determines  $\alpha$ ; the complication is that the 'edge' velocity is given by (4.13), and determination of that value of  $\alpha$  from direct integration of (4.13) is impossible. However, the integral may be found directly from (4.8), by dividing the equation by  $\delta v_e$  and then integrating, which results in

$$2\lambda \int_0^t \delta v_e(\tau) d\tau = 2(1 - 2\lambda)t - \frac{4\lambda\gamma}{\omega} \sin(\omega t) + \log \left( \frac{\delta v_e(t)}{\delta v_e(0)} \right). \quad (4.23)$$

For the range  $\lambda < 1/2$ , one can show by direct substitution of the long-time behaviour from (4.9) that the log term in (4.23) just cancels the first two terms of the right-hand side of that equation, so in fact the integral vanishes as  $t \rightarrow \infty$ , recovering (4.5) for the 'edge' velocity, and the value of  $\alpha$  already obtained for this case in (4.22).

In the situation for which  $\lambda > 1/2$ , substitution of (4.13) into the log term in (4.23) leads to the equation

$$2\lambda \int_0^t \delta v_e(\tau) d\tau = 2(1 - 2\lambda)t + \log \left( \frac{F(0)}{F(t)} \right). \quad (4.24)$$

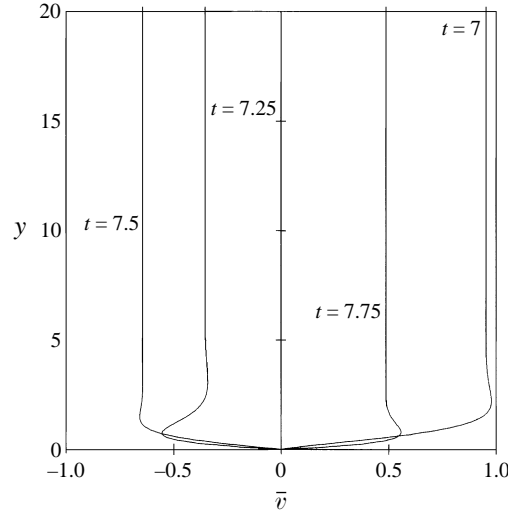


FIGURE 4. Rear-stagnation-point self-similar solutions at 0, 1/4, 1/2, and 3/4 points in the cycle, for  $\lambda = 0.90$ ,  $\gamma = 0.90$  and  $\omega = 2\pi$ .

Letting  $t \rightarrow \infty$  leads to the required integral,

$$\int_0^t \bar{v}_e(\tau) d\tau \sim \frac{1-\lambda}{\lambda} t + O(1), \quad (4.25)$$

which result is (surprisingly) valid for all  $\gamma$ ! Substitution into (4.20) and putting to the coefficient of  $t$  in the exponential leads to the proper value for  $\alpha$ ,

$$\alpha = \frac{1-2\lambda}{1-\lambda}, \quad (4.26)$$

which agrees with the steady solution results, and is now seen to be valid for all values of  $\gamma$ . Note that (4.25) also indicates that the mean value of  $\delta\bar{v}_e$  approaches an average value of  $(1-\lambda)/\lambda$  for  $t \rightarrow \infty$ , a result which agrees with the numerics described in §5 below. This result passes the self-consistency check for the asymptotics shown here, namely that  $\alpha < 0$ , which is clearly true according to (4.26). Finally, the numerical results from §4.4 and also from §5 are entirely consistent with this value.

#### 4.4. Numerical integration of the equations

To numerically verify the existence of a similarity solution at the rear stagnation point, the exact similarity equation was solved in each range of  $\lambda$  for  $|\gamma| < 1$  and  $\omega = 2\pi$ . The numerical problem was formulated as an exact perturbation about the steady flow. A logarithmic coordinate transformation (Canuto *et al.* 1988) was used in the  $y$ -direction to capture the algebraic decay of  $\phi$  while maintaining sufficient resolution near the wall. This transformation worked well except for  $\lambda = 1/2$ , where the near-logarithmic decay of  $\phi$  made it difficult to both capture the boundary layer and resolve the wall region. Second-order central differences were used in the  $y$ -direction and second-order backward differences were used in the  $t$ -direction. The steady flow was used as the initial condition and the solution was marched in time to  $t = 8$ , which was sufficient to reach the long-time periodic behaviour. Two grids were used in the numerical solution:  $N_y \times N_t = 500 \times 800$  and  $1000 \times 1600$ . The results were improved with Richardson extrapolation.



In order to solve the exact similarity equation for  $1/2 < \lambda < 1$ , the exact plateau velocity is required, so (4.6) is numerically integrated to obtain that edge condition; this is simpler for computational purposes than actually using results (4.10)–(4.13). The numerical solution of the similarity equation verifies that a similarity solution can be found for  $\lambda < 1$ ,  $\gamma < 1$ ,  $\omega = 2\pi$ . Figure 4 shows typical numerical results at the 0, 1/4, 1/2, and 3/4 points of the last oscillatory cycle, and includes a reversing plateau velocity.

In the next section, the complete quarter-layer equations are integrated numerically to determine the boundary in the  $\gamma, \lambda$  parameter space where an unsteady breakdown in the solution occurs.

## 5. Numerical integration of the quarter-layer equations

When not restricted to an asymptotic limit, numerical methods are required to solve the quarter-layer equations. The choice of a computational coordinate system is of paramount importance for this numerical problem. The choice of numerical discretization is also crucial in obtaining good numerical results.

### 5.1. Solution of the steady equations

We know from the large- $\omega$  asymptotics that the steady solution dominates the outer part of the boundary layer, so we take advantage by generating the grid for the unsteady problem using the steady equations. The presence of a singularity at  $x = \pi$  for  $1/2 \leq \lambda \leq 1$  necessitates the use of a grid transformation to capture the rapid thickening of the boundary layer as the rear stagnation point is approached. In preliminary attempts to solve the equations, we tried a simple  $x$ -independent  $y$ -grid stretching for the unsteady equations. Previously, Page (1985) had used a simple  $x$ -dependent  $y$ -grid stretching for the steady equations. Neither transformation was completely satisfactory in the region  $\pi - x \ll 1$  for  $\lambda$  near 1. A better transformation for the steady equations is given by Page & Cowley (1988), who used a modified Von Mises (mVM) transformation based on the stream function  $\psi$  that eliminates the Von Mises singularity at the wall and front stagnation point. In addition to capturing the boundary layer, this transformation has the advantage of eliminating  $u$  from the steady momentum equation, decoupling momentum from continuity. This is a major simplification analytically, since one fewer equation must be solved, and numerically, since  $u$  becomes unbounded as  $y \rightarrow \infty$ .

The generalization of mVM to the unsteady case is not very useful. Most importantly, if the oscillation is large enough so that the flow reverses,  $\psi$  is negative and  $y$  is a double-valued function of  $\psi$  in the region of flow reversal. Thus, the unsteady mVM is a good transformation only if  $\gamma$  is less than the value required for periodic flow reversal, which restricts  $\gamma$  in an undesirable manner. Instead, we utilized mVM to first solve the steady problem and then used the steady solution to generate the grid transformation  $\eta(x, y)$  for the unsteady problem. This transformation has the advantage of producing the correct growth as  $x \rightarrow \pi$  without needlessly restricting  $\gamma$ . A shortcoming of mVM, however, is that it fails to resolve the wall region as  $x \rightarrow \pi$ . Page & Cowley (1988) overcame this problem with unequal step sizes in  $\eta$ , a procedure that we believe is too cumbersome for the unsteady problem.

In searching for a better coordinate transformation, we ultimately abandoned mVM in favour of a transformation utilizing the large- $y$  asymptotics of the steady equation

(cf. Page & Cowley 1988; Buckmaster 1969)

$$1 - \frac{v(y_{max}(x))}{v_e} = e' = \frac{A_\infty}{\cos^5(x/2)} y_{max}^{-(3+1/\lambda)} \exp(-\lambda(y_{max}(x) - \delta^*(x))^2 \cos^2(x/2)), \quad (5.1)$$

where  $e'$ ,  $A_\infty$ , and  $y_{max}(x=0)$  are determined by analysing the numerical solution of the front-stagnation-point similarity solution as  $y \rightarrow \infty$ . They are all functions of  $\lambda$ . The numerical solutions of the steady equations are insensitive to the precise value of  $A_\infty$ , which is very difficult to obtain accurately.

We define the computational coordinate  $\eta(x, y)$  in two stages. First, we scale out the boundary-layer growth  $y_{max}(x)$ ,

$$\bar{y}(x, y) \equiv \frac{y}{y_{max}(x)}, \quad 0 \leq \bar{y} \leq 1. \quad (5.2)$$

We then move the coordinate points to resolve the wall region near  $x = \pi$ , without overdepleting the points in the edge region, and retain a uniform grid near  $x = 0$ , where grid stretching is unnecessary:

$$\bar{y} = \eta \left[ \left( \frac{y_{max}(0)}{y_{max}(x)} \right) \left( e^{-\alpha\eta^\beta} - e^{-\alpha} f(\eta) \right) + f(\eta) \right], \quad 0 \leq \eta \leq 1, \quad (5.3)$$

$$f(\eta) = \frac{1 - e^{-\alpha\eta^\beta}}{1 - e^{-\alpha}}, \quad (5.4)$$

where  $\alpha$  and  $\beta$  are control parameters.

In solving the steady equations, we obtained the best results by formulating the velocities as perturbations about their edge behaviour:

$$\bar{v}_0 = 1 - \frac{v}{v_e}, \quad \bar{u}_0 = y \frac{dv_e}{dx} + u. \quad (5.5)$$

By scaling the velocity by  $v_e$ , the initial condition is no longer  $v = 0$  at  $x = 0$ . Instead, we obtain the initial condition by solving the front-stagnation-point similarity solution.

To integrate the steady equations, we use  $O(\Delta\eta^2)$  central differences to reduce the steady partial differential equations to a large system of ordinary differential equations in the usual method-of-lines approach. We then integrate the system of ordinary differential equations forward in  $x$  with an extrapolation scheme based on the implicit Euler method (Hairer & Wanner 1991). The scheme is variable step size and variable-order to control the errors in the  $x$ -direction (relative error tolerance  $R_{TOL} = 10^{-7}$  specified). The method works very well and produces results that agree with the previous work on the steady problem. The integration includes many more  $x$ -steps than could possibly be used in the unsteady problem, and uses irregular step sizes as well. To compensate, the code was written to save the coordinate and velocity data only at given increments of  $x$ , which were then used in the unsteady problem. A typical grid, for  $\lambda = 0.9$ , is shown in figure 5. Since the grid is generated from the physically relevant steady equations, the grid contains the same singular growth at the rear stagnation point contained in the boundary-layer solution. This singular behaviour is nicely captured in figure 5.

The steady solution is also used to generate the initial conditions for the unsteady problem. We use the uniformly-valid-in- $y$  high-frequency approximation that follows from (3.24), (3.31). This initial condition works well and minimizes the time to reach the long-time solution of the unsteady equations.

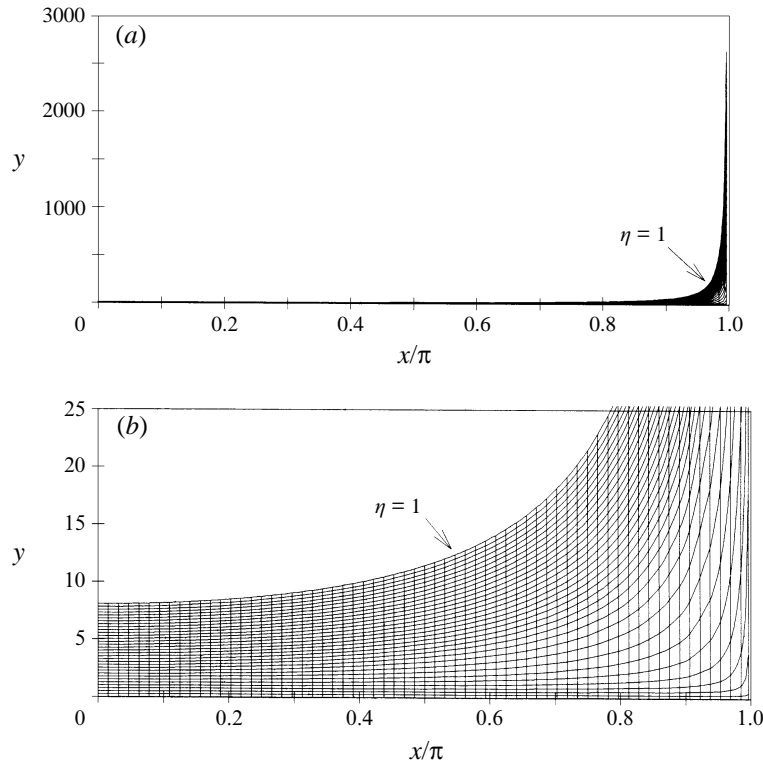


FIGURE 5.  $256 \times 256$ -point grid generated from the steady solution for  $\lambda = 0.9$  (not all grid points plotted): (a) the singular growth of the grid (and boundary layer) as one nears the rear stagnation point at  $x/\pi = 1$ ; (b) a close-up of the grid nearer to the wall.

### 5.2. Solution of the unsteady equations

The numerical solution of the unsteady equations is difficult to obtain – harder than one might at first suppose. The complicated singularity structure at  $x = \pi$  disrupts the numerical solution away from  $x = \pi$ , especially when there is significant flow reversal. For  $\lambda < 1/2$ , almost any stable consistent integration scheme works, but for  $\lambda > 0.75$ , the ability to get any numerical solution depends critically on the choice of discretization.

We formulate the equations in the  $x, \eta$ -coordinates generated by the steady solution. The velocities are again written as perturbations about the edge velocity

$$\bar{v} = v - v_e, \quad \bar{u} = y \frac{\partial v_e}{\partial x} + u. \quad (5.6)$$

By not scaling the velocity  $v$  by the edge velocity as in the steady equation, we can use boundary condition (2.12).

We discretize the governing partial differential equations with the method-of-lines approach. We tried virtually every finite-difference spatial discretization imaginable. The only discretization that was stable enough for  $\lambda > 0.75$  utilizes second-order central differences for the diffusion term and second-order upwind differences for both the  $x$  and the  $\eta$  convective terms. Using upwind differences in the  $\eta$ -term is the crucial step toward a sufficiently stable method. Adjacent to the wall and edge,  $\eta$ -upwind differences have to be replaced by central differences, to no ill-effect.

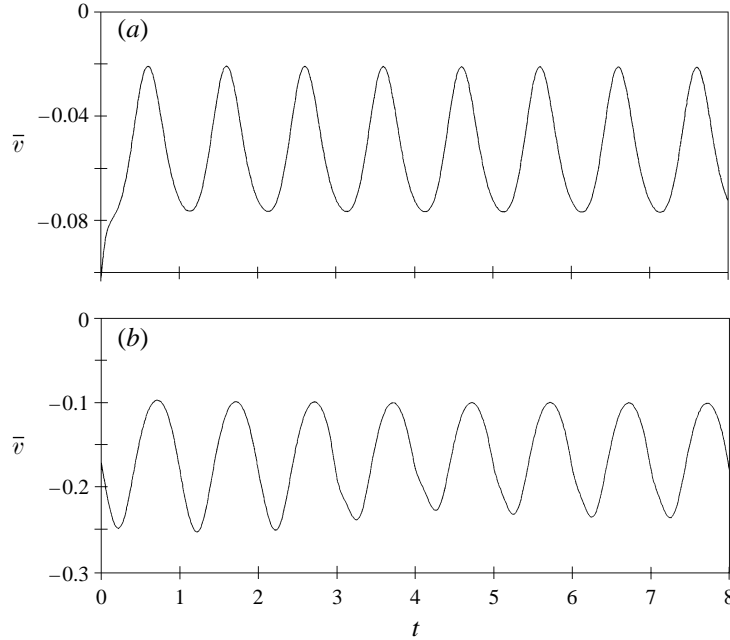


FIGURE 6. Time history for the velocity component parallel to the wall, at a location near the wall, for  $\lambda = 0.9, \gamma = 0.9$  and  $\omega = 2\pi$ : (a) near the front stagnation point (at  $x = 1/32, \eta = 1/16$ ), (b) near the rear stagnation point (at  $x = 31/32, \eta = 1/4$ ). The initial condition is the high-frequency asymptotic solution given in §3.

The continuity equation is discretized by solving for  $u$  as an integral of  $v$  and then evaluating the integral with the trapezoidal rule. This effectively eliminates  $u$  as an unknown, so that only the momentum equation remains.

We integrate the discretized momentum equation using an extrapolation scheme based on the linearly implicit Euler scheme (Hairer & Wanner 1991). (The scheme is fully implicit for the steady equation.) In the integration, we use not the exact Jacobian, but only the Jacobian terms that result from the discretized diffusion term. In this way, the Jacobian is tridiagonal and does not change in time, which leads to efficient solution of the equations. Since the scheme is only linearly implicit, no iteration is required. The apparent cost of linear-implicitness is that the scheme is not unconditionally stable, but requires a CFL-like condition on  $\Delta t$ . On the other hand, the program uses step size and order control to efficiently solve the equations using  $R_{TOL} = 10^{-6}$  as the relative error tolerance.

### 5.3. Numerical results

Although the temporal errors are controlled automatically by the computer program, we still must determine the spatial-grid spacing. Starting with a  $32 \times 32$  grid, after successively doubling the number of grid points in each direction until reaching a  $256 \times 256$  grid, we determined that the velocities are accurate to three places, with better accuracy achieved for smaller  $\lambda$  and/or smaller  $x$ . Excessive execution time limits us to the  $256 \times 256$  grid.

With an adequate grid spacing determined, the next question is how many time steps are required to reach the long-time behaviour. Figure 6 shows the unsteady behaviour at two points in the boundary layer for  $\lambda = 0.90, \gamma = 0.9, \omega = 2\pi$ . The

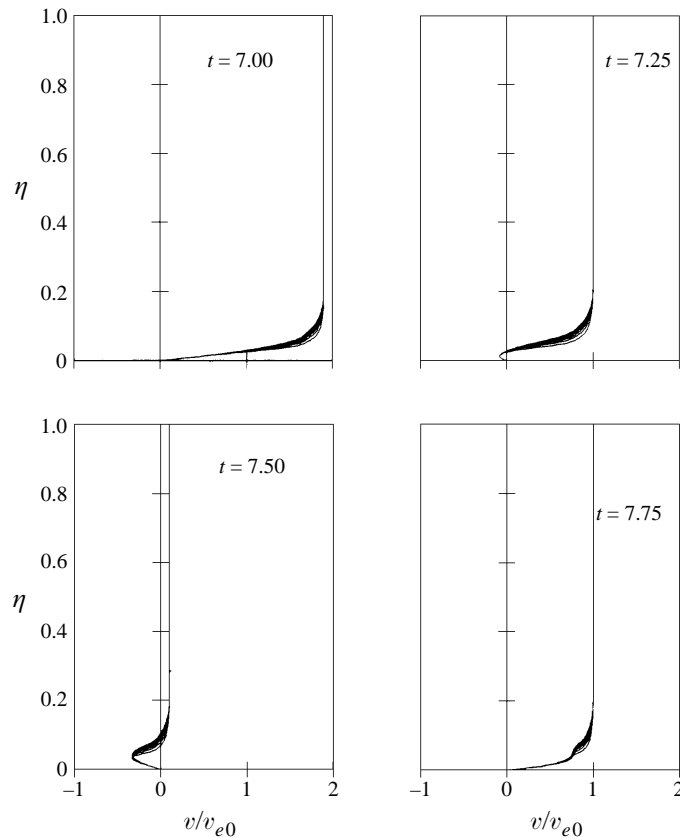


FIGURE 7. Velocity profiles near the rear stagnation point, at 0, 1/4, 1/2 and 3/4 points in the cycle. The final profile (the thickest) is at  $x/\pi = 1 - 1/256$ , and the previous ones are at successive 1/256 steps forward of this location. The results are shown scaled; the actual boundary layer is growing dramatically in  $y$ . For this case,  $\lambda = 0.40$ ,  $\gamma = 0.90$  and  $\omega = 2\pi$ .

first location at  $x = 1/32$ ,  $\eta = 1/16$  is near the front stagnation point and near the wall. At this location, diffusion effects are high and the upstream flow is virtually free of initial transients. As a result, a very regular long-time oscillatory behaviour is established after about 1/2 of a cycle (figure 6a). Near the rear stagnation point at  $x = 31/32$ ,  $\eta = 1/4$ , the situation is more complicated. At this location, there is significant grid stretching, so that  $\eta = 1/4$  is quite far from the wall (in fact, this location is within the free shear layer connecting the plateau velocity to the edge velocity). Furthermore, transients from upstream pass through this point as they are advected downstream. If we examine figure 6(b) carefully, we see that the velocity begins with one type of periodic behaviour. Then, between  $t = 2$  and  $t = 3$ , disturbances kick the system out of the initial periodic solution and the velocity latches onto its long-time periodic solution. The transients have sufficiently decayed by about  $t = 7$  to 8, to make it possible to treat the last cycle as the long-time periodic solution.

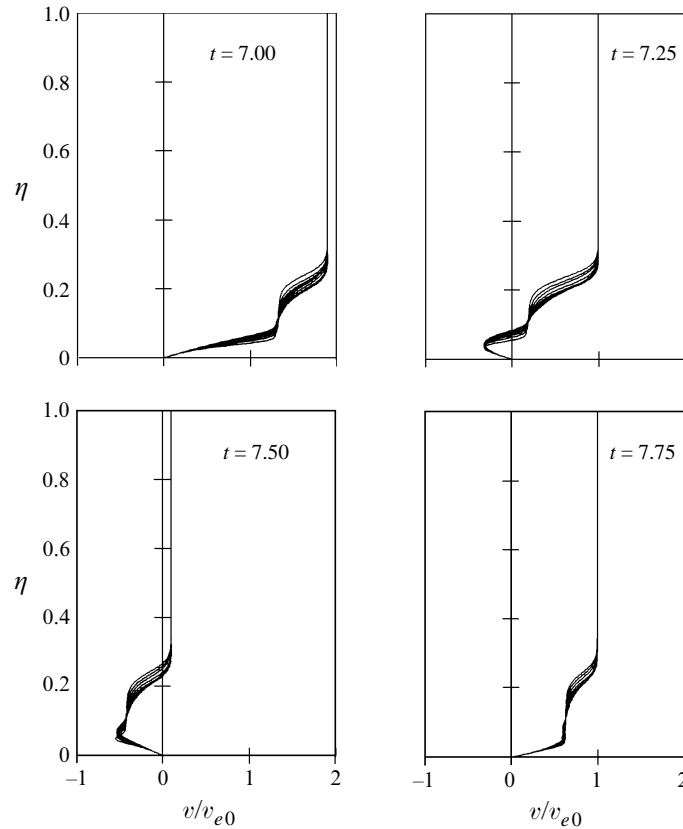


FIGURE 8. As figure 7 but for  $\lambda = 0.70$ ,  $\gamma = 0.90$  and  $\omega = 2\pi$ .

We discuss below the results obtained from integrating the equations for a variety of  $0 < \lambda < 1$ ,  $0 < \gamma < 1$ ,  $\omega = 2\pi$ . For the grid control parameters, we found  $\alpha = 85$ ,  $\beta = 3$  to be adequate for all the physical parameter values. Figure 7 presents the last eight velocity profiles (normalized by the steady part of the edge velocity) at the 0, 1/4, 1/2, and 3/4 times in the oscillation cycle for  $\lambda = 0.40$ ,  $\gamma = 0.90$ , at  $x/\pi = 248/256, \dots, 255/256$  (with mesh parameters  $A_\infty = 30.43$  and  $y_{max}(x = 0) = 23.3$ , see (5.1)). Since this value of  $\lambda$  is less than 1/2, there is no plateau and the velocity profiles all have the usual boundary-layer profile appearance. The figure clearly shows the periodic behaviour of the velocity profiles and includes periodic flow reversal. We also note that the velocity does not overshoot the edge velocity.

The second case shown here is one for which  $\lambda = 0.70$ ,  $\gamma = 0.90$ , with parameters  $A_\infty = 0.5904$  and  $y_{max}(x = 0) = 9.08$  (figure 8). Here, we clearly see the lower, plateau, and free-shear-layer regions of the boundary layer. The lower region and plateau region are in excellent agreement with the rear-stagnation-point similarity solution. This value of  $\gamma$  is sufficiently large to cause the entire plateau region to periodically reverse, so that the region of reversed flow can become quite large. The lower-region profiles can show considerable overshoot of the plateau velocity, a condition absent in the steady problem. The velocity does not, however, overshoot the edge velocity. Note that the distance from the free shear layer to the wall does not change appreciably during the cycle for this value of  $\lambda$ .

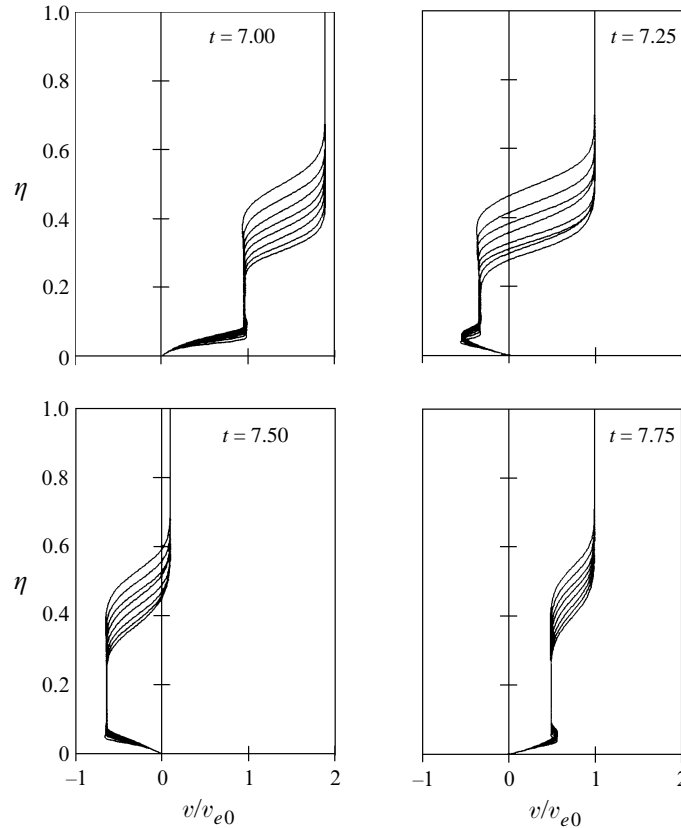


FIGURE 9. As figure 7 but for  $\lambda = 0.90$ ,  $\gamma = 0.90$  and  $\omega = 2\pi$ .

Figure 9 shows the results for  $\lambda = 0.90$ ,  $\gamma = 0.90$ , with parameters  $A_\infty = 0.3696$  and  $y_{max}(x = 0) = 7.76$ . Note that  $y_{max}(x = 0)$  has been decreasing as  $\lambda$  increases because the increased advection thins the boundary layer near the front stagnation point as it greatly increases the boundary layer thickness near the rear stagnation point. Once again, the boundary layer shows the lower, plateau, and free-shear-layer structure. The lower region and plateau region are also in excellent agreement with the rear-stagnation-point similarity solution, figure 4.

The parameter space is mapped out in figure 10. We include therein critical  $\gamma(\lambda)$  curves (at  $\omega = 2\pi$ ) for periodic flow reversal at the rear stagnation point, periodic flow reversal at the front stagnation point, periodic flow reversal of the edge velocity, periodic flow reversal of the plateau velocity, as well as the line  $\lambda = 1/2$  which divides the stable edge velocity (4.5) from the stable plateau velocity (4.13) for the similarity solution, and the line  $\lambda = 1$ , which is the upper limit on stable solutions.

## 6. High-frequency solutions for full cylinder

To this point, we have taken the oscillation frequency to be low, in particular of order  $\Omega E^{1/2}$ . In this section, we turn briefly to the case for which the frequency,  $\omega'$ , is in fact of order  $\Omega$ . It turns out that many of the details are very similar to those found in §3.3, so some of the analysis will not be repeated here.

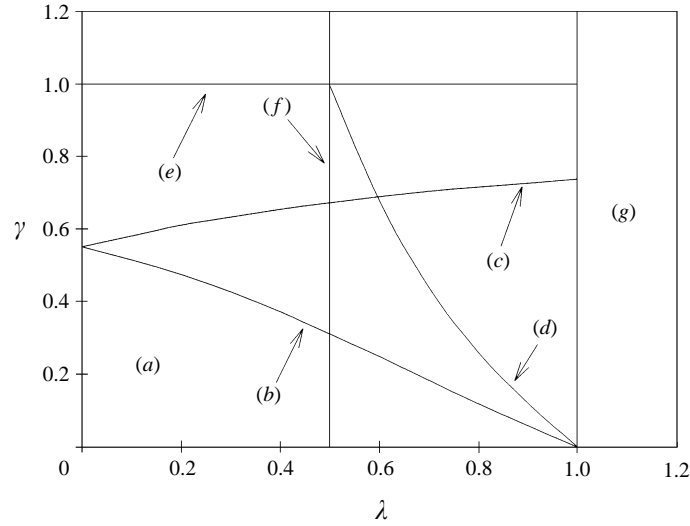


FIGURE 10. The  $\gamma$ ,  $\lambda$  parameter space for  $\omega = 2\pi$ . (a) region of no flow reversal, (b) minimum  $\gamma$  for periodic flow reversal at the rear stagnation point, (c) minimum  $\gamma$  for periodic flow reversal at the front stagnation point, (d) minimum  $\gamma$  for periodic reversal of the plateau velocity, (e) minimum  $\gamma$  for periodic reversal of the edge velocity, (f) minimum  $\lambda$  for a stable plateau velocity, (g) no stable solution.

What happens is that, as  $\omega$  increases through larger and larger values, the thinner lower partition of the quarter layer in §3.4 eventually, as  $\omega'$  finally attains  $O(\Omega)$ , takes thickness  $E^{1/2}$ , in a layer distinct from the quasi-steady quarter layer above it. In this Section, we examine briefly some elements of the flow for such a case.

We define the time,  $t' = \hat{t}/\Omega$ , and the frequency,  $\omega'$ , is written as  $\omega' = \Omega\hat{\omega}$ . In this case, the equations of motion and boundary conditions remain (2.2)–(2.5), except that the time term in (2.3) is replaced by  $\partial\mathbf{u}/\partial\hat{t}$ . Proceeding to the outer expansion, we write  $\mathbf{u} = \mathbf{u}_0 + E^{1/4}\mathbf{u}_1 + E^{1/2}\mathbf{u}_2 + \dots$ . Substitution into (2.2) and (2.3) leads to the following result:

$$\frac{\partial^2}{\partial\hat{t}^2} \nabla^2 p_n + \left( \frac{\partial^2}{\partial\hat{t}^2} + 4 \right) \frac{\partial^2 p_n}{\partial z^2} = 0 \quad \text{for } n \leq 2, \quad (6.1)$$

and  $(u_n, v_n)$  are simply related to  $p_n$ . If the cylindrical obstacle spans the entire gap between the plates, then the interior flow is  $z$ -independent, since the boundary conditions are  $z$ -independent. In that case,  $\partial p_n/\partial z \equiv 0$  for all  $z$ , and so (6.1) reduces, for a time-periodic state, to

$$\nabla_1^2 p_n = 0, \quad (6.2)$$

where  $\nabla_1^2$  is an horizontal Laplacian. In that case, the outer solution for  $n = 0$  is, again, the classical flow past a circular cylinder, and the leading-order edge velocity for the boundary layer(s) on the surface is given by (2.9) again. Therefore,

$$v \rightarrow 2 \sin(x)(1 + \gamma \cos(\hat{\omega}\hat{t})) \quad \text{at the layer edge.} \quad (6.3)$$



## 6.1. The quarter layer

In the usual fashion described earlier, the equation valid in the quarter layer may be derived. As in §2, we put  $r - a = E^{1/4}y$  into (2.2)–(2.3), and the result is

$$\frac{\partial v}{\partial x} + \frac{\partial u}{\partial y} + \frac{E^{1/4}}{a} \frac{\partial}{\partial y}(y u) = 0, \quad (6.4)$$

$$\begin{aligned} \frac{\partial v}{\partial \hat{t}} + E^{1/2} \lambda \left( v \frac{\partial v}{\partial x} + u \frac{\partial v}{\partial y} \right) + 2E^{1/2} \left( [v - v^{(p)}] + \frac{v^{(p)}}{(1 + \hat{\omega}/2)^{1/2}} \right) &= \frac{\partial v_e}{\partial \hat{t}} \\ + E^{1/2} \lambda v_e \frac{\partial v_e}{\partial x} + 2E^{1/2} \left( [v_e - v_e^{(p)}] + \frac{v_e^{(p)}}{(1 + \hat{\omega}/2)^{1/2}} \right) + E^{1/2} \frac{\partial^2 v}{\partial y^2}, & \quad (6.5) \end{aligned}$$

where  $v^{(p)}$  denotes the oscillatory portion of  $v$ , which has zero mean. The third term on each side of this equation takes a quite different form from that in equation (2.7), for the case for small  $\omega'/\Omega$ . The reason is that the periodic portion of the velocity at the Ekman layer's edge leads to a different Ekman suction law. Since the Ekman layer is linear in this parameter range, unlike the quarter layer, the oscillatory and non-oscillatory suction laws may simply be added, and what is shown in the third term of (6.5) reflects both elements of that Ekman suction. It turns out, as we shall see below, that this modification of the stretching term has no leading-order effect on the flow in the quarter layer.

The asymptotic expansion in this layer then proceeds as

$$(u, v) = (u_0, v_0) + E^{1/4}(u_1, v_1) + E^{1/2}(u_2, v_2) + \dots \quad (6.6)$$

Substitution into (6.4), (6.5) leads to the equation

$$\frac{\partial}{\partial \hat{t}}(v_0 - v_{0e}) = 0. \quad (6.7)$$

The only solution to this equation that can satisfy the boundary conditions is given by

$$\left. \begin{aligned} v_0 = v_e^{(p)}(x, t) + V_0(x, y), \quad u_0 = -y v_{e_x}^{(p)} + U_0(x, y), \\ v_e^{(p)} = 2\gamma \sin(x) \cos(\hat{\omega} \hat{t}), \end{aligned} \right\} \quad (6.8)$$

which is essentially identical to the decomposition adopted in (3.30).

The next term in the series for  $v$ , namely  $v_1$ , satisfies the same equation (6.7). As we shall see in §6.3, the matching condition for  $v_1$  for  $y \rightarrow \infty$  is that  $v_1$  approach a function of  $x$  alone – there is no time dependence. Therefore, the integral of (6.7) for  $v_1$  is simply  $v_1 = v_1(x, y) \equiv V_1(x, y)$ . Combined with the continuity equation for  $(u_1, v_1)$ , derived from (6.4), it is easily shown that the second-order radial velocity component in the quarter layer is given by

$$u_1 = \frac{y^2}{a} \frac{\partial v_e^{(p)}}{\partial x} + U_1(x, y) + u_{1,w}(x, \hat{t}) \quad \text{and} \quad U_1(x, 0) = 0. \quad (6.9)$$

It turns out that the equations obeyed by  $(U_1, V_1)$  are steady state; they are not written down here for brevity. A bit more will be said in §6.3 about their solution.

A careful examination of the boundary-layer structure on  $r = a+$  in this parameter range reveals that the familiar ‘one-third layer’ of steady flow is absent; the distinguished limit disappears because of the largeness of the unsteady term. It is replaced by another distinguished limit: a Stokes layer. A first thought would suggest that a one-third layer remains, to connect to the steady portion of  $v$ ; however, even though

the outer, quarter layer is essentially steady, the oscillatory component,  $v_e^{(p)}$  in (6.8), is passed through the layer unchanged, so any layers beneath the quarter layer see an unsteady ‘outer’ flow to which to match. Hence, the matching below the quarter layer is to the Stokes layer, and there is no ‘one-third’ layer. As a referee has suggested, things change in the limit  $\gamma \rightarrow 0$ ; for  $\gamma$  sufficiently small, the outer layer is truly steady, and the one-third layer scale is recovered. We have not explored that limit here, and in this Section,  $\gamma = O(1)$  – which assures the absence of the one-third layer.

Therefore, as in §3.4, to match to the layer below the quarter layer, we expand this solution for small  $y$ . Since the thinner layer in this case has a width proportional to  $E^{1/2}$ , we write  $r - a = E^{1/2}Z$ , so clearly  $y = E^{1/4}Z$ . Utilizing a Taylor series evaluation of (6.6) near  $y = 0$ , and making a change of variable, we obtain the matching condition for the thin layer beneath the quarter layer. Thus,

$$v \sim v_e^{(p)} + V_{0y}(x, 0)E^{1/4}Z + E^{1/2} [v_2(x, 0) + V_{1y}(x, 0)Z + \frac{1}{2}V_{0yy}(x, 0)Z^2] + \dots \quad (6.10)$$

### 6.2. The Stokes layer

The layer beneath the quarter layer is a Stokes layer, and substitution into (2.3) leads to the following equation:

$$\mathcal{R}(v) = E^{1/2} \mathcal{N}(v), \quad \mathcal{R}(v) \equiv \frac{\partial v}{\partial \hat{t}} - \frac{\partial^2 v}{\partial Z^2}, \quad (6.11)$$

where  $\mathcal{N}$  is a nonlinear operator. An asymptotic expansion

$$v = v^{(0)}(x, Z, \hat{t}) + E^{1/4}v^{(1)}(x, Z, \hat{t}) + E^{1/2}v^{(2)}(x, Z, \hat{t}) + \dots, \quad (6.12)$$

substituted into (6.11) leads to  $\mathcal{R}(v^{(0)}) = 0$ , and its solution is

$$v^{(0)} = 2\gamma \sin(x) \operatorname{Re} \left( e^{i\hat{\omega}\hat{t}} (1 - e^{-(i\hat{\omega})^{1/2}Z}) \right). \quad (6.13)$$

The next term,  $v^{(1)}$ , satisfies the same equation,  $\mathcal{R}(v^{(1)}) = 0$ , and the solution is, by matching to (6.10), easily seen to be given by

$$v^{(1)} = V_0(x, 0)Z. \quad (6.14)$$

The next term involves the nonlinear operator  $\mathcal{N}$ , and is not included here, since it is very like the analysis in §3.4.

The leading-order radial velocity component in the Stokes layer,  $u^{(0)}$ , may then be determined from the scaled continuity equation. Rewriting the  $Z \rightarrow \infty$  limit of that radial velocity in quarter-layer variables leads to

$$u \sim -2\gamma\pi \cos(x) [y \cos(\hat{\omega}\hat{t}) - E^{1/4}\hat{\omega}^{-1/2} \cos(\hat{\omega}\hat{t} - \pi/4)] \quad \text{for } y \rightarrow \infty. \quad (6.15)$$

Matching to the quarter-layer asymptotic series and using (6.9) then determines  $u_{1,w}$  to be given by

$$u_{1,w} = -2\gamma \cos(x)\hat{\omega}^{-1/2} \cos(\hat{\omega}\hat{t} - \pi/4). \quad (6.16)$$

### 6.3. Higher-order outer flow

The solution for higher-order terms in the outer region, away from the boundary layers, determines the effects of those layers on the outer flow. The effects will be small, but this is the way in which rectification would appear in this formulation. Consistent with the velocity expansion noted early in this section, the velocity potential, which is harmonic (see (6.2)), has the following asymptotic expansion:

$$\phi = \phi_0(r, \theta, t) + E^{1/4}\phi_1(r, \theta) + E^{1/2}\phi_2(r, \theta, t) + \dots \quad (6.17)$$

The first term is, of course, the circular-cylinder flow already utilized, for which the unsteadiness is simply a multiplier. We must now look into the detailed matching to the quarter layer to deduce boundary conditions on  $\phi_1$  and  $\phi_2$ . The equations for  $(U_0, V_0)$  and  $(U_1, V_1)$  lead to the following behaviour for  $u_r$ , the radial velocity, at the quarter-layer edge ( $y \rightarrow \infty$ ), which must match to the outer flow:

$$\begin{aligned} \pi u_r \sim u_0 E^{1/4} \left[ 1 - E^{1/4} \frac{y}{a} \right] - E^{1/2} \frac{\partial}{\partial x} \int_0^\infty (v_1 - v_{1e}) \, dy \\ + E^{1/2} u_{1,w}(x, \hat{t}) - E^{1/2} y \frac{\partial v_{1e}}{\partial x} + o(E^{1/2}), \end{aligned} \quad (6.18a)$$

$$u_0 \sim -y \frac{\partial v_e^{(s)}}{\partial x} - \frac{\partial}{\partial x} \int_0^\infty (V_0 - v_e^{(s)}) \, dy, \quad (6.18b)$$

where the (s) superscript refers to the non-oscillatory component of  $v_e$ . Most of the details of the matching can be worked out easily and are not included here. In summary, in matching  $u$  to  $\partial\phi/\partial r$ , a number of terms arising out of the Taylor expansion of  $\partial\phi/\partial r$  on  $r = a$  match to terms proportional to  $y$  and  $y^2$  in (6.18). Apart from those, the following conditions emerge:

$$\frac{\partial\phi_0}{\partial r} = 0 \quad \text{at } r = a, \quad (6.19a)$$

$$a \frac{\partial\phi_1}{\partial r} = -\frac{\partial}{\partial x} \int_0^\infty (V_0 - v_e^{(s)}) \, dy, \quad (6.19b)$$

$$a \frac{\partial\phi_2}{\partial r} = -\frac{\partial}{\partial x} \int_0^\infty (v_1 - v_{1e}) \, dy + u_{1,w}. \quad (6.19c)$$

The first term clearly determines the familiar function for flow past a circular cylinder,  $\phi_0$ , as discussed earlier in the paper and used throughout. The quarter-layer solution allows the right-hand side of (6.19b) to be worked out, and so  $\phi_1$  can be entirely determined. Thus, the quantity  $v_1 = (1/r)\partial\phi_1/\partial\theta$  at  $r = a$  is non-zero; it leads to the non-zero edge condition for  $v_1$  in the quarter layer. In fact, since the right-hand side of (6.19b) is clearly steady, the result for  $\phi_1$  is identical to that worked out by Walker & Stewartson (1972) for steady flow. Hence, in this parameter range, effects of the interaction of unsteadiness with the topography cannot occur at  $O(E^{1/4})$ , but not until  $O(E^{1/2})$  – as is evident from (6.19c). The function  $\phi_2$  cannot be written down by hand, since the integral involved in (6.19c) must be obtained from our numerical solution of the quarter-layer equations. However, it is clear from the form of (6.19c) that the ‘inflow’ at the layer edge which drives the  $\phi_2$  solution is the sum of a steady component – determined entirely from the steady  $(u_1, v_1)$  quarter-layer solution – and an oscillatory component arising in the Stokes layer,  $u_{1,w}$ , which is given precisely by (6.16). Thus, if we make the decomposition

$$\phi_2 = \phi_2^{(s)}(r, \theta) + \phi_2^{(p)}(r, \theta, \hat{t}), \quad (6.20)$$

then the unsteady portion of this high-order solution is

$$\phi_2^{(p)} = -\frac{2\gamma \cos\theta}{\hat{\omega}^{1/2}} \cos(\hat{\omega}\hat{t} - \pi/4) \frac{a^2}{r}. \quad (6.21)$$

While there is clearly an  $\frac{1}{8}$ th cycle phase lag in this third term, at these high frequencies the unsteadiness seems inconsequential. There is no rectification, and clearly, since  $\phi_2^{(s)}$

can be shown to be odd in  $\theta$  – and so  $v_2^{(s)}$  is even – there is no evidence of any left–right asymmetry of the kind reported by Boyer & Zhang (1990*b*) in their experiments.

## 7. Discussion

Our goal has been to determine the range of  $\lambda$  and  $\gamma$  for which the quarter-layer equations have a solution. Beginning with the analytical results, we found in §3.1 that the edge velocity is a stable solution of the infinite- $\gamma$  limit of the governing equations only if  $\lambda < 1$  (independent of  $\gamma$ ), indicating that a solution of the equations cannot satisfy the boundary conditions for  $\lambda > 1$ . Furthermore, in §3.4, we found that the large- $\omega$  limit of the equations is essentially the steady solution plus a Stokes layer adjacent to the wall, so that the leading-order solution exists for all  $\lambda < 1$ .

Second, our investigation of the rear-stagnation-point similarity solution indicates that the similarity solution satisfies the usual edge velocity for  $\lambda < 1/2$ , independent of the value of  $\gamma$ . We found that a time-periodic velocity ‘plateau’ arises at the similarity solution’s ‘edge’ for values of  $\lambda$  between  $1/2$  and  $1$ , and that the plateau velocity itself is a stable solution of the infinite- $\gamma$  limit of the similarity equations. On the other hand, further investigation of the large- $\gamma$  behaviour of the solutions indicates that a finite-time singularity may arise at the rear stagnation point for sufficiently large edge perturbations for all  $\lambda > 0$ , but such large perturbations may be rare in practice.

Our numerical solutions of the full quarter-layer equations indeed verify that long-time periodic solutions exist, and that the solution structure near the rear stagnation point consists of a lower shear layer and plateau region (which are in complete agreement with the similarity solution) and a free shear layer that connects the plateau region to the free-stream flow. These numerical solutions support our theoretical conclusion that the quarter-layer equations have solutions for  $\lambda < 1$  and that this critical  $\lambda$  is independent of  $\gamma$  and  $\omega$ .

Finally, we noted briefly that, for the case of a full-height cylinder, the surface boundary layer splits into an essentially steady quarter layer and a thinner Stokes layer – so the rear-stagnation-point behaviour is presumably just that of steady flow.

The experiments reported by Boyer & Zhang (1990*b*) are directly relevant to this work. Though the bulk of the flow visualization images shown are for  $\omega'/\Omega = 2$ , rather than the small values of  $\omega'/\Omega$  studied here (for short cylinders), there is a noticeable discrepancy between our results and those experiments: the visualizations plainly show a strong left–right asymmetry, part of which is due to rectification, and for which there is no evidence in the results reported here, either for the low-frequency problem of §§3–5 or the full-cylinder  $O(1)$  frequency results of §6. Generally, the experiments were run at Rossby numbers well beyond values for which this theory is valid, i.e. for  $\lambda$  well beyond  $1$ . Neither does the solution for separated flow past a cylinder given by Page (1987) for  $\lambda = O(1)$  show any evidence of such asymmetry. Secondly, for obstacles that do not span the entire gap between the plates, the only results given here are for small values of  $\omega'/\Omega$ . The combination of non-full-height obstacles and larger frequencies makes the outer flow quite different and very possibly asymmetric. So, further theoretical investigation is required to discover the reasons for such disagreement.

The rectification issue requires a bit more discussion. In the paper by Walker & Stewartson (1974) on homogeneous slow flow past an hemisphere, there is an asymmetry that arises at higher order in the outer flow, which is induced by vortex

stretching over the hemisphere in the interior shear layer. No such higher-order asymmetry is seen in the similar flow past a right circular cylinder (Foster 1972). Since the mechanism of rectification seems to be vortex stretching (Zimmerman 1980), no flap-topped bump in the range  $\epsilon = O(E^{1/2})$  could exhibit that, since the Taylor–Proudman theorem prohibits fluid columns from upstream from passing over the top of the bump. We suspect that a repeat of this analysis, for say an hemisphere or a cone, would show evidence of rectification, though it will be small because  $\epsilon$  is small.

The authors are grateful to Dr Peter Duck for several helpful discussions about this problem, and to the referees, each of whom provided several helpful clarifications, including, from one referee, a correction to the form of (6.5).

### Appendix. The $v_1$ correction for $\lambda \ll 1$

The small- $\lambda$  regular perturbation solution is discussed in §3, with the results for the first term in the (3.7) series given there. Substitution of (3.7) into (2.7), (2.8) leads to the equations satisfied by  $(u_1, v_1)$ ; the solution for  $v_1$  is in the form

$$v_1 = 2\pi \sin(2\pi x)(v_h + v_p), \quad (\text{A } 1)$$

where

$$v_h = -K_0 e^{-\sqrt{2}y} - e^{-Ay} [K_1 \cos(\omega t - By) + K_2 \sin(\omega t - By)] \\ - e^{-A_2 y} [K_3 \cos(2\omega t - B_2 y) + K_4 \sin(2\omega t - B_2 y)], \quad (\text{A } 2)$$

and

$$v_p = e^{-\sqrt{2}y} \left[ \frac{y}{4} \left( y + \frac{3}{\sqrt{2}} \right) + \frac{\gamma}{\omega} \left( C_0 \cos(\omega t) + (\sqrt{2}y + C_1) \sin(\omega t) \right) \right] \\ + e^{-Ay} \left[ \gamma^2 \left[ \frac{1}{A^2 + B^2} \left( \frac{1}{2} \cos(By) - \frac{1}{\omega} \sin(By) \right) \right. \right. \\ + \frac{2}{\omega} \left( \frac{2}{\omega} \cos(\omega t - By) - \frac{5}{4} \sin(\omega t - By) \right) \cos(\omega t) \\ + \frac{2}{\omega} \left( \left( \frac{Ay}{2} + \frac{3}{4} \right) \cos(\omega t - By) - \frac{By}{2} \sin(\omega t - By) \right) \sin(\omega t) \left. \right] \\ + \gamma \left( y \left( \frac{y}{4} + C_2 \right) \cos(\omega t - By) + C_3 y \sin(\omega t - By) \right) \left. \right] \\ + \gamma^2 e^{-2Ay} \left[ C_4 + \frac{1}{18 + 2\omega^2} (3 \cos(2(\omega t - By)) + \omega \sin(2(\omega t - By))) \right] \\ + \gamma e^{-(A+\sqrt{2})y} [C_5 \cos(\omega t - By) + C_6 \sin(\omega t - By)]. \quad (\text{A } 3)$$

The various constants in this solution are then given by

$$A_2 = \text{Re}((2 + 2i\omega)^{1/2}) = ((1 + \omega^2)^{1/2} + 1)^{1/2}, \quad (\text{A } 4a)$$

$$B_2 = \text{Im}((2 + 2i\omega)^{1/2}) = ((1 + \omega^2)^{1/2} - 1)^{1/2}, \quad (\text{A } 4b)$$

$$C_0 = \frac{4}{\omega} + \frac{\sqrt{2}B}{A^2 + B^2}, \quad C_1 = 2 - \frac{\sqrt{2}A}{A^2 + B^2}, \quad (\text{A } 5a, b)$$

$$C_2 = \frac{5}{4} \frac{A}{A^2 + B^2} - \frac{1}{2\sqrt{2}}, \quad C_3 = \frac{5}{4} \frac{B}{A^2 + B^2}, \quad (\text{A } 5c, d)$$

$$C_4 = \frac{1}{2(2A^2 - 1)} \left[ \frac{1}{2} + \frac{1}{A^2 + B^2} \right], \quad (\text{A } 5e)$$

$$C_5 = \frac{2A(\sqrt{2}A + 1) - (A^2/\sqrt{2} + A + \sqrt{2}) (1/\sqrt{2} + \sqrt{2}/(A^2 + B^2))}{2(\sqrt{2}A + 1)^2 + B^2}, \quad (\text{A } 5f)$$

$$C_6 = \frac{\omega/\sqrt{2} - (B + 3\omega/2\sqrt{2}) (1/\sqrt{2} + \sqrt{2}/(A^2 + B^2))}{2(\sqrt{2}A + 1)^2 + B^2}, \quad (\text{A } 5g)$$

$$K_0 = \gamma^2 \left[ \frac{1}{2(A^2 + B^2)} + \frac{2}{\omega^2} + C_4 \right], \quad (\text{A } 6a)$$

$$K_2 = \gamma \left[ \frac{C_1}{\omega} + C_6 \right], \quad (\text{A } 6b, c)$$

$$K_3 = \gamma^2 \left[ \frac{3}{18 + 2\omega^2} + \frac{2}{\omega^2} \right], \quad K_4 = \gamma^2 \left[ \frac{\omega}{18 + 2\omega^2} - \frac{1}{2\omega} \right]. \quad (\text{A } 6d, e)$$

## REFERENCES

- BAINES, H. & DAVIES, P. A. 1980 Topographic effects in rotating and stratified fluids. In *Orographic Effects in Planetary Flows* (ed. P. W. White & R. Hide). GARP Publications Ser. 23, pp. 233–299. Geneva: World Meteorological Organization.
- BARCILON, V. 1970 Some inertial modifications of the linear viscous theory of steady rotating fluid flows *Phys. Fluids* **13**, 537.
- BOYER, D. L., DAVIES, P. A. & HOLLAND, W. R. 1984 Rotating flow past discs and cylindrical depressions. *J. Fluid Mech.* **141**, 67.
- BOYER, D. L., DAVIES, P. A., HOLLAND, W. R., BIOLLEY, F. & HONJI, H. 1987 Stratified rotating flow over and around isolated three-dimensional topography. *Phil. Trans. R. Soc. Lond. A* **322**, 213.
- BOYER, D. L., D'HIERES, G., DIDELLE, H., VERRON, J., CHEN, R. & TAO, L. 1991 Laboratory simulation of tidal rectification over seamounts; homogeneous model. *J. Phys. Oceanogr.* **21**, 1559.
- BOYER, D. & ZHANG, X. 1990a The interaction of time-dependent rotating and stratified flow with isolated topography. *Dyn. Atmos. Oceans* **14**, 543.
- BOYER, D. & ZHANG, X. 1990b Motion of oscillatory currents past isolated topography. *J. Phys. Oceanogr.* **20**, 1425.
- BUCKMASTER, J. 1969 Separation and magnetohydrodynamics. *J. Fluid Mech.* **38**, 481.
- BUCKMASTER, J. 1971 Boundary-layer structure at a magnetohydrodynamic rear stagnation point. *Q. Mech. Appl. Maths J.* **24**, 373.
- CANUTO, C., HUSSAINI, M. Y., QUARTERONI, A. & ZANG, T. A. 1988 *Spectral Methods in Fluid Dynamics*. Springer.
- FOSTER, M. R. 1972 The flow caused by the differential rotation of a right circular cylindrical depression in one of two rapidly rotating parallel planes. *J. Fluid Mech.* **53**, 647.
- FOSTER, M. R. 1989 Rotating and stratified flow past a steep-sided obstacle. Incipient separation. *J. Fluid Mech.* **206**, 47.

- GENIN, A., DAYTON, P., LONSDALE, P. & SPIESS, F. 1986 Corals on seamount peaks provide evidence of current acceleration over deep-sea topography. *Nature* **322**, 59.
- GOULD, W., HENDRY, R. & HUPPERT, H. 1981 An abyssal topographic experiment. *Deep-Sea Res.* **28A**, 409.
- HAIRER, E. & WANNER, G. 1991 *Solving Ordinary Differential Equations II*. Springer.
- HOGG, N. G. 1973 On the stratified Taylor column. *J. Fluid Mech.* **58**, 517.
- HUDSPETH, R. T. 1991 Significance of the Keulegan–Carpenter parameter. *J. Hydraul. Engng* **117**, 1626.
- HUPPERT, H. & BRYAN, K. 1976 Topographically generated eddies. *Deep-Sea Res.* **23**, 655.
- JACOBS, S. J. 1964 The Taylor column problem. *J. Fluid Mech.* **20**, 581.
- KEULEGAN, G. H. & CARPENTER, L. H. 1958 Forces on cylinders and plates in an oscillating fluid. *J. Res. Natl Bur. Stand* **60**, 423.
- KUNKA, M. D. 1991 The effects of free-stream oscillation on the flow over a cylinder in a rotating frame. MS Thesis, The Ohio State University.
- LEIBOVICH, S. 1967 Magneto-hydrodynamic flow at a rear stagnation point. *J. Fluid Mech.* **19**, 401.
- MOORE, D. W. & SAFFMAN, P. G. 1969 The structure of free vertical shear layers in a rotating fluid and the motion produced by a slowly rising body. *Phil. Trans. R. Soc. Lond. A* **264**, 597.
- OWENS, W. & HOGG, N. G. 1980 Oceanic observations of stratified Taylor columns near a bump. *Deep-Sea Res.* **27A**, 1029.
- PAGE, M. 1985 On the low-Rossby number flow of a rotating fluid past a circular cylinder. *J. Fluid Mech.* **156**, 205.
- PAGE, M. 1987 Separated and free-streamline flows in a rotating fluid at low Rossby number. *J. Fluid Mech.* **179**, 155.
- PAGE, M. & COWLEY, S. 1988 On the rotating-fluid flow near the rear stagnation point of a circular cylinder. *J. Fluid Mech.* **154**, 79.
- PROUDMAN, I. 1956 The almost rigid rotation of viscous fluid between concentric spheres. *J. Fluid Mech.* **1**, 505.
- STEWARTSON, K. 1957 On almost rigid rotations. *J. Fluid Mech.* **3**, 17.
- STEWARTSON, K. 1966 On almost rigid rotations. Part 2. *J. Fluid Mech.* **26**, 131.
- STOCKER, J. R., DUCK, P. W. & PAGE, M. A. 1997 On the unsteady low-Rossby number flow of a rotating fluid past a circular cylinder. *Phys. Fluids* **9**, 600.
- TAYLOR, G. I. 1923 Experiments on the motion of solid bodies through rotating fluids. *Proc. R. Soc. Lond. A* **104**, 213.
- TELIONIS, D. P. 1981 *Unsteady Viscous Flows*. Springer.
- VERRON, J. 1986 Topographic eddies in temporally varying oceanic flows. *Geophys. Astrophys. Fluid Dyn.* **35**, 257.
- WALKER, J. D. A. & STEWARTSON, K. 1972 The flow past a circular cylinder in a rotating frame. *Z. Angew. Math. Phys.* **23**, 745.
- WALKER, J. D. A. & STEWARTSON, K. 1974 The Taylor column problem for a hemisphere. *J. Fluid Mech.* **66**, 767.
- XU, Y., BOYER, D. L. & ZHANG, X. 1993 Rotating oscillatory flow past a cylinder. *Phys. Fluids A* **5**, 868.
- ZHANG, X. & BOYER, D. L. 1993 Laboratory study of rotating, stratified oscillatory flow over a seamount. *J. Phys. Oceanogr.* **23**, 1122.
- ZIMMERMAN, J. T. F. 1980 Vorticity transfer by tidal currents over an irregular topography. *J. Marine Res.* **38**, 601.